

Dynamic modelling and evaluation of preclinical trials in acute leukaemia

Julian Wäsche¹, Romina Ludwig^{2,3}, Irmela Jeremias^{2,3,4},
Christiane Fuchs^{1,5*}

¹Data Science Group, Faculty of Business Administration and Economics, Bielefeld University, Bielefeld, Germany.

²Research Unit Apoptosis in Hematopoietic Stem Cells, Helmholtz Munich, German Research Center for Environmental Health (HMGU), Munich, Germany.

³Department of Pediatrics, Dr. von Hauner Children's Hospital, University Hospital, LMU Munich, Munich, Germany.

⁴German Cancer Consortium (DKTK), partner site Munich, a partnership between DKFZ and University Hospital LMU Munich, Munich, Germany.

⁵Institute of Computational Biology, Computational Health Center, Helmholtz Munich, Neuherberg, Germany.

*Corresponding author(s). E-mail(s): christiane.fuchs@uni-bielefeld.de;

Abstract

Dynamic models are widely used to mathematically describe biological phenomena that evolve over time. One important area of application is leukaemia research, where leukaemia cells are genetically modified in preclinical studies to explore new therapeutic targets for reducing leukaemic burden. In advanced experiments, these studies are often conducted in mice and generate time-resolved data, the analysis of which may reveal growth-inhibiting effects of the investigated gene modifications. However, the experimental data is often times evaluated using statistical tests which compare measurements from only two different time points. This approach does not only reduce the time series to two instances but also neglects biological knowledge about cell mechanisms. Such knowledge, translated into mathematical models, expands the power to investigate and understand effects of modifications on underlying mechanisms based on experimental data. We utilise two population growth models – an exponential and a logistic growth model – to capture cell dynamics over the whole experimental time horizon and to consider all measurement times jointly. This approach enables us to derive modification effects from estimated model parameters. We demonstrate that the exponential growth model recognises simulated scenarios more reliably than the other candidate model and than a statistical test. Moreover, we apply the population growth models to evaluate the efficacy of candidate gene knockouts in patient-derived xenograft (PDX) models of acute leukaemia.

Keywords: Ordinary differential equation, Population growth model, Profile likelihood, Acute leukaemia, CRISPR-Cas9 screen

1 Introduction

Ordinary differential equations (ODEs) are suitable to mathematically represent mechanistic knowledge about processes of cells and biological systems in general ([Bang and Villaverde, 2025](#)). This model-based approach allows researchers to validate their understanding of the system of interest and to study its characteristics for time-resolved data by inferring model parameters. Model parameters also allow them to quantify effects of interventions in the system.

An important area where ODE modelling shows potential is cancer research, for instance, in drug development. A major class of targeted cancer drugs is characterised by reducing the net growth of cancer cell populations by either inhibiting proliferation (thus cell division) or stimulating cell death for malignant cells. Developing drugs in this class is particularly challenging, especially in the early stages of research. Many therapeutic targets are explored, but they must pass several phases before they can reach clinical application. One crucial stage is preclinical trials. Here, relevant data about cell population growth-inhibiting effects is collected, including trials with laboratory animals.

In this work, we focus on preclinical experiments testing potential new therapeutic targets for acute leukaemia. Even though the mortality rate of acute leukaemia patients has decreased substantially over the past decades, leukaemia is still one of the main causes of death in children ([Siegel et al, 2023](#)). To identify therapeutic targets, primary patient cells are engrafted into immune compromised NOD scid gamma (NSG) mice (NOD mice were originally used to study type 1 diabetes). After successful engraftment, PDX cells are isolated from mice and can be genetically modified using, for example, the CRISPR-Cas9 (clustered regularly interspaced short palindromic repeats and CRISPR-associated protein 9) method ([Wang et al, 2014; Shalem et al, 2014](#)). In particular, certain genes that are suspected to be relevant for proliferation or survival are knocked out ([Bahrami et al, 2023; Ghalandary et al, 2023](#)). These cells are engrafted into NSG mice together with an untreated control population. Such PDX models constitute mouse models in which tumour cells can be studied

in the environment of a living organism. Compared to cell cultures, these models better represent the growth environment of tumours in humans (Hidalgo et al, 2014; Gao et al, 2015). At an advanced stage with a high blast load, a mouse needs to be sacrificed to measure the concentration of modified leukaemia cells in the bone marrow. This time point is sample-specific and may vary for different leukaemia samples used in the experiments. The output measurements are compared to the input concentrations, i.e. the proportions of the engrafted modified cells, to examine possible growth-inhibiting effects of the gene modification. An effective gene modification can have a proliferation-inhibiting or a cell death-stimulating effect. The essential steps of this kind of experiments are illustrated in Figure 1 in a simplified manner.

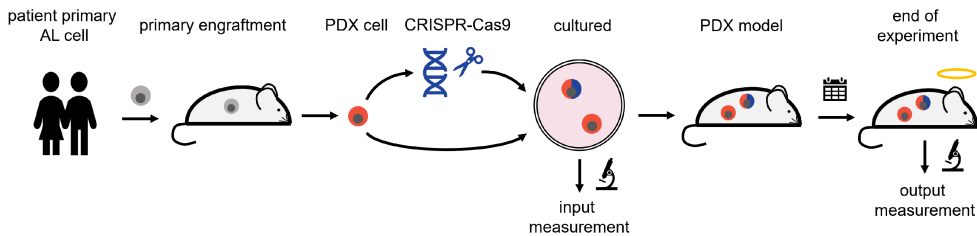


Fig. 1: Schematic workflow of gene modification experiments, here a CRISPR-Cas9 knockout experiment, exploring new therapeutic targets for acute leukaemia (AL). First, patient cells are engrafted into mice to generate PDX cells. These cells are genetically modified and again engrafted into mice together with an untreated cell population providing PDX models. The output measurements, i.e. the concentrations of the modified population in the bone marrow of mice at an advanced stage of leukaemia, are compared with the input measurements, i.e. the concentration that is injected, to assess a possible growth-inhibiting effect on the modified cell population

The standard approach to compare the input and output relations is to apply a statistical hypothesis test, e.g. a paired *t*-test, to assess whether the measurements at these two time points differ significantly from each other. This approach neglects mechanistic knowledge about cell reactions, such as proliferation, death and interactions, that are potentially affected by gene modifications and on the basis of which effects can be assessed. Moreover, this approach only compares output measurements from one time point with the corresponding inputs from day 0. The experiments on which this work is based, however, have up to two measurement times for output values. Therefore, up to two *t*-tests are required to evaluate them separately, although the measurements share the same experimental conditions (with different output times). This separation of evaluations induces small sample sizes for single paired *t*-tests, and so a sufficient number of measurements is required to detect a possible effect of a

gene modification. As one mouse needs to be sacrificed for every single output measurement, researchers face a trade-off between the information content of experiments and ethical and financial considerations. Thus, the paired *t*-test approach ends up compounding challenges for efficient evaluation of preclinical leukaemia trials.

In this work, we provide a model-based approach for the evaluation of gene modification experiments on leukaemia cells that overcomes several limitations of the standard testing approach. We mathematically represent the series of cell events using ODE models to describe the dynamics of cell populations. In particular, we apply two common population growth models, an exponential and a logistic growth model (Kuang et al, 2016). A population growth model is incorporated in the recently developed algorithm Chronos (Dempster et al, 2021) to evaluate CRISPR-Cas9 knockout screens. Chronos describes single-guide RNA (sgRNA) depletion using an exponential growth model. It has outperformed other common algorithms in the evaluation of knockout screens, such as MAGeCK (Li et al, 2014, 2015) and CERES (Meyers et al, 2017), especially when time-series data is available (Dempster et al, 2021). However, exponential growth of a population is often unrealistic in the long run, as it implies a constant doubling time and that population sizes either tend towards infinity or zero (e.g. Kuang et al, 2016). Therefore, we compare its performance with a logistic growth model involving an upper limit for population sizes. Logistic growth models have already been applied successfully to describe the growth of leukaemia cell populations (e.g. Ebinger et al, 2016; Hoffmann et al, 2020; Chulián et al, 2022). For both models, population dynamics are characterised by parameters. To estimate these parameters, we employ the set of all experimental measurements taken at several output times to capture population dynamics over the entire experimental time horizon. Furthermore, we investigate parameter identifiability and derive confidence intervals for relevant parameters by means of profile likelihoods (Raue et al, 2009, 2010). Based on estimated parameters and confidence intervals, we investigate growth-inhibiting effects of gene modifications.

We show that the exponential growth model outperforms the logistic growth model in the evaluation of various simulated scenarios in a simulation study, especially for small sample sizes. A paired *t*-test for late output measurements can compete with the population growth models in detecting modification effects, at least for this specific allocation of measurement times of the considered type of experiments and for a sufficiently large sample size. For experimental data of gene modification experiments, the

growth models and the paired t -test for late measurement times yield similar evaluation results. Nonetheless, the exponential growth model provides a more informative approach to analyse underlying dynamics and its parameters can be more reliably inferred than those of the logistic growth model.

This article is organised as follows: Section 2 introduces the exponential and the logistic growth model as well as the observable model. In Section 3, we delineate statistical methods, such as maximum likelihood estimation and profile likelihoods, and we define two notions of parameter identifiability. We examine structural identifiability of the growth models, introduce evaluation methods and compare the evaluation performance of the growth models with paired t -tests for simulated scenarios in Section 4. In Section 5, we analyse a series of CRISPR-Cas9 knockout experiments in PDX models of acute leukaemia. A discussion and conclusion follows in Section 6.

2 Dynamic growth models

Biological systems evolving over time are often mathematically described by ODEs. We consider two-dimensional ODE systems for the gene modification experiments with state variable vector $\mathbf{x}(t) = (x_1(t), x_2(t))^T$ representing the leukaemia cell numbers of both the modified ($x_1(t)$) and the untreated ($x_2(t)$) population at time $t \geq 0$. At any time, cells of both populations can perform one out of two reactions: they can either grow and divide (proliferation) or die (apoptosis). These two possible reactions determine the dynamics of population numbers. To describe the dynamics formally, we examine two growth models that are both embedded into the broad class of ODEs defined by

$$d\mathbf{x}(t) = \mathbf{f}(\mathbf{x}(t), \boldsymbol{\theta})dt, \quad \mathbf{x}(0) \in \mathbb{R}^2. \quad (1)$$

The concrete choice of the \mathbb{R}^2 -valued function \mathbf{f} depends on the considered growth model. The function \mathbf{f} is parametrised by a parameter vector $\boldsymbol{\theta} \in \mathbb{R}^p$, the value of which is either specified by the modeller, or it is estimated from data. The vector $\boldsymbol{\theta}$ may also contain the initial conditions $\mathbf{x}(0) = (x_1(0), x_2(0))^T$ of the state variable \mathbf{x} if these are unknown.

The state variable components $x_k(t)$, $k = 1, 2$, are \mathbb{R} -valued quantities, whereas the number of cells for the modification experiments are integers. In the application considered here, cell numbers range from 10^4 to 10^9 . These scales can be regarded as

sufficiently large to treat the trajectory of cell numbers as approximately continuous on a macroscopic level such that an ODE representation is appropriate to impose.

In the following, we introduce an exponential and a logistic growth model to characterise the growth of the two cell populations within the gene modification experiments. These two models are widely used to mathematically describe the growth of cancer (e.g. [Kuang et al, 2016](#)) as well as the growth of populations in general (e.g. [Kot, 2001](#)). Moreover, we define the observable model that represents the form of the experimental measurements. We simulate both the trajectories of the ODE systems and the observables with the simulation framework of the `dMod` package (Version 1.0.2, [Kaschek et al, 2019](#)) in R.

2.1 Exponential growth model

We assume that the per capita net growth rate of cells from Population k is given by the parameter $\beta_k \in \mathbb{R}$ for $k = 1, 2$. The parameter reflects the difference of the per capita proliferation rate and the death rate of the population. The resulting dynamics of the cell population numbers are represented by the ODE system

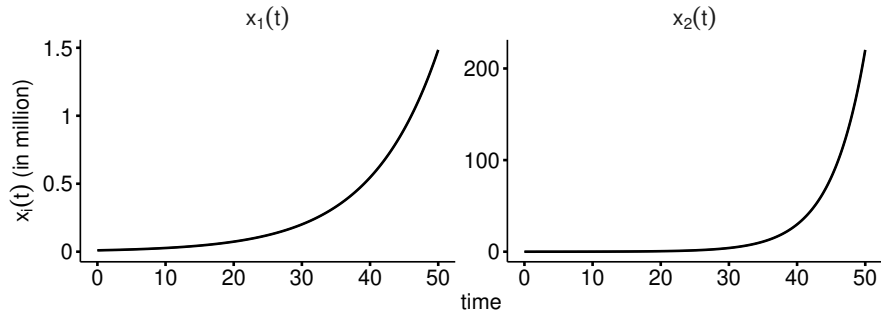
$$\begin{aligned} dx_1(t) &= \beta_1 x_1(t) dt, & x_1(0) &\in \mathbb{R}, \\ dx_2(t) &= \beta_2 x_2(t) dt, & x_2(0) &\in \mathbb{R}. \end{aligned} \tag{2}$$

The system (2) admits the analytic solution

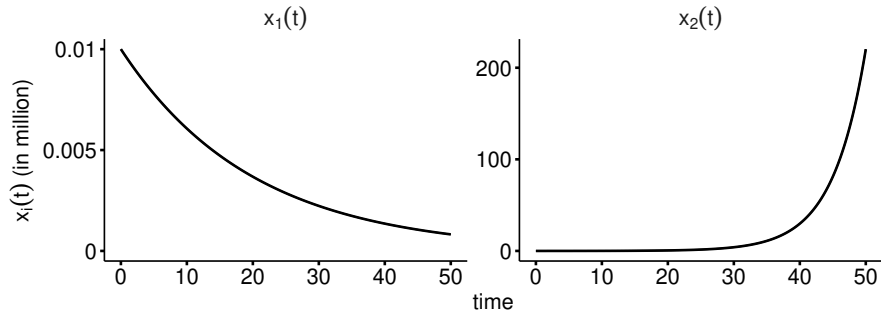
$$x_1(t) = x_1(0)e^{\beta_1 t}, \quad x_2(t) = x_2(0)e^{\beta_2 t}, \quad t \geq 0. \tag{3}$$

The solution in Equation (3) shows that, if $\beta_k > 0$, Population k grows exponentially and, if $\beta_k < 0$, it declines exponentially. In the application considered in this article, scientists seek after gene modifications that make Population 1 grow less strongly or even shrink in comparison to Population 2, i. e. $\beta_1 < \beta_2$. These two desirable cases are depicted in Figure 2 for exemplary parameter values.

The exponential nature in Equation (3) implies that $x_k(t) \rightarrow \infty$ if $\beta_k > 0$, or $x_k(t) \rightarrow 0$ if $\beta_k < 0$, as $t \rightarrow \infty$. Both this asymptotic behaviour and a constant doubling time are rarely observed in real phenomena in the long run. At some point, for example, food resources or the space in the system are exhausted such that growth



(a) $\beta_1 = 0.1, \beta_2 = 0.2$



(b) $\beta_1 = -0.05, \beta_2 = 0.2$

Fig. 2: Trajectories of the exponential growth model with exemplary values for β_1 and β_2 with $x_1(0) = x_2(0) = 10^4$. (a) Both populations grow, as $\beta_1, \beta_2 > 0$, but Population 1 grows less strongly than Population 2. (b) Population 1 shrinks and Population 2 grows, as $\beta_1 < 0$ and $\beta_2 > 0$

decelerates (e.g. [Kuang et al, 2016](#)). In our application, however, we are more interested in the evaluation of population dynamics on a relatively small time horizon than in predicting beyond this horizon. It has been observed that exponential growth of a population in a limited time period can be reasonably assumed (e.g. [Kuang et al, 2016](#)). Thus, it still makes sense to employ the exponential growth model. In addition, however, we will investigate the logistic growth model which takes into account an upper bound for population sizes.

2.2 Logistic growth model

A logistic growth model accounts for the fact that real-world populations rarely grow permanently exponentially. It assumes that the sum of all system entities cannot exceed a carrying capacity $K \in \mathbb{N}$ at any time t if the sum of the initial conditions is less than K , i.e. $x_1(0) + x_2(0) < K$ in our case. In the considered context, the capacity K reflects the finite resources for leukaemia cells to proliferate in the bone marrow of mice and we presume that the bone marrow can only absorb a maximum

of K leukaemia cells. The corresponding logistic growth model reads

$$\begin{aligned} dx_1(t) &= \lambda_1 \left(1 - \frac{x_1(t) + x_2(t)}{K} \right) x_1(t) dt, \quad x_1(0) \in \mathbb{R}, \\ dx_2(t) &= \lambda_2 \left(1 - \frac{x_1(t) + x_2(t)}{K} \right) x_2(t) dt, \quad x_2(0) \in \mathbb{R}, \end{aligned} \quad (4)$$

for net growth rates $\lambda_1, \lambda_2 \in \mathbb{R}$ of Population 1 and Population 2, respectively. As the initial conditions usually satisfy $x_1(0) + x_2(0) < K$, Population k grows if $\lambda_k > 0$, and, if $\lambda_k < 0$, the population size declines. If $x_1(t) + x_2(t) \ll K$ for small t , the term in the brackets in (4) is close to one and the number of cells grows (or declines) almost exponentially. The closer the sum $x_1(t) + x_2(t)$ approaches the threshold K for larger t , the stronger the growth (or decay) decelerates until it reaches a steady state. The value of the steady state depends on the values of the parameters λ_1, λ_2 and K and the initial conditions $x_1(0)$ and $x_2(0)$. So, the shared capacity links the behaviour of both cell populations, and the growth of both populations depends on the other's growth activity. An analytically explicit solution like (3) is unavailable for (4). For parameter values of a less strongly growing as well as a shrinking Population 1, simulated model trajectories are shown in Figure 3.

2.3 Observable model

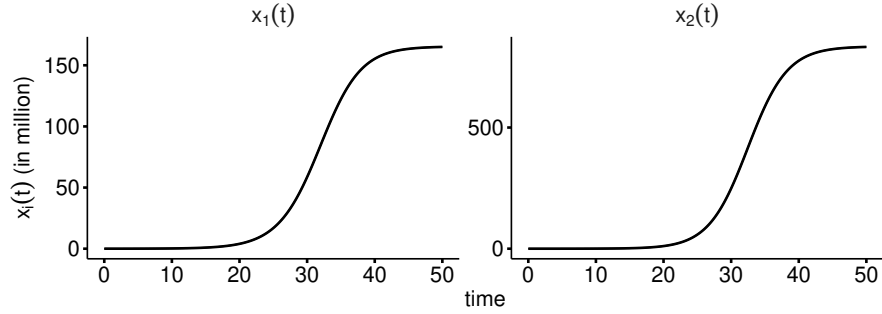
For gene modification experiments, it is technically difficult to measure absolute population sizes, i.e. $x_1(t)$ and $x_2(t)$, explicitly. Therefore, it is common to measure the concentration of one population in relation to the total number of cells of both populations. The observable for both growth models thus results as

$$\eta(t) = \frac{x_1(t)}{x_1(t) + x_2(t)}, \quad t \geq 0. \quad (5)$$

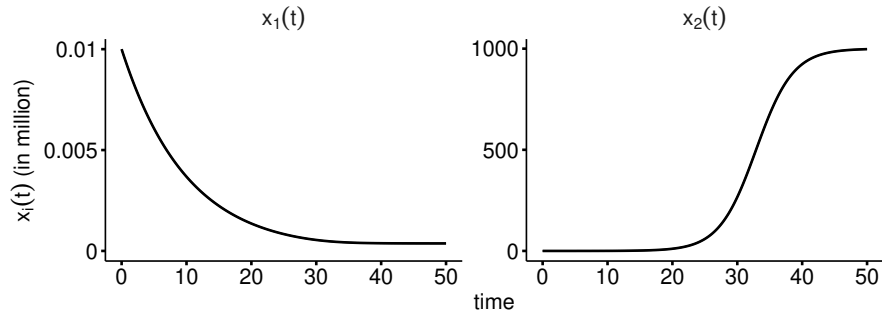
For the exponential growth model (2), we can rewrite Equation (5) and plug in (3) such that we obtain

$$\eta(t) = \frac{1}{1 + \frac{x_2(t)}{x_1(t)}} = \frac{1}{1 + \frac{x_2(0)}{x_1(0)} e^{(\beta_2 - \beta_1)t}}, \quad t \geq 0. \quad (6)$$

Trajectories of the observable are depicted in Figure 4 for the dynamics of the exponential and the logistic growth model from Figure 2a and Figure 3a, respectively. In Figure 4a, the relative amount of Population 1 tends to zero due to the exponential



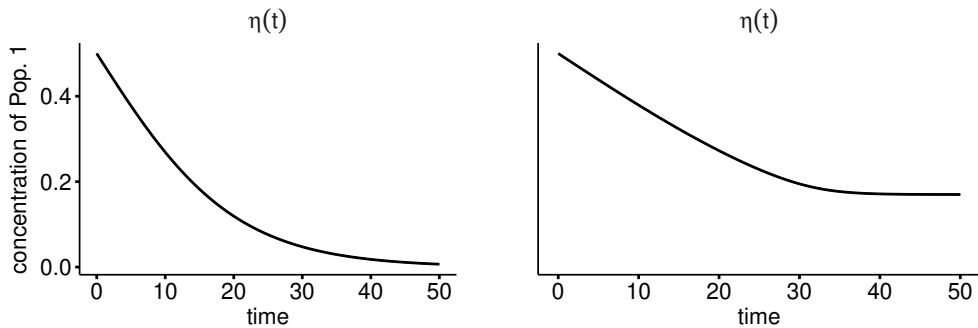
(a) $\lambda_1 = 0.3, \lambda_2 = 0.35$



(b) $\lambda_1 = -0.1, \lambda_2 = 0.35$

Fig. 3: Trajectories of the logistic growth model with exemplary values for λ_1 and λ_2 with $K = 10^9$ and $x_1(0) = x_2(0) = 10^4$. (a) Both populations grow, as $\lambda_1, \lambda_2 > 0$, but Population 1 grows less strongly than Population 2. (b) Population 1 shrinks and Population 2 grows, as $\lambda_1 < 0$ and $\lambda_2 > 0$

nature of the model, whereas the observable reaches a steady state around 0.15 in the long run in Figure 4b.



(a) Exponential growth, $\beta_1 = 0.1, \beta_2 = 0.2$

(b) Logistic growth, $\lambda_1 = 0.3, \lambda_2 = 0.35$

Fig. 4: Trajectories of the observable $\eta(t)$ for (a) the exponential and (b) the logistic growth model with $x_1(0) = x_2(0) = 10^4$ and $K = 10^9$. The other parameter values correspond to those in Figures 2a and 3a

3 Statistical inference

A mathematical model attempts to depict real mechanisms so that insights can be transferred from the model to reality. The values of model parameters can sometimes be determined by the modeller on the basis of knowledge from the specific discipline. In the case of the gene modification experiments considered here, neither the parameter values nor the initial conditions are exactly known. The goal of statistical inference is to estimate these values based on measurements and to study resulting properties. However, models are only an idealized representation of reality. Measurements naturally deviate from the modelled observable $\eta(t)$ as they are, for example, subject to biological stochasticity and experimental noise. We regard measurements $y(t)$ for both growth models as realisations of the random variable

$$Y(t) = \eta(t) \cdot \varepsilon(t) = \frac{x_1(t)}{x_1(t) + x_2(t)} \cdot \varepsilon(t), \quad t \geq 0, \quad (7)$$

where $\varepsilon(t) \sim \mathcal{LN}\left(-\frac{\sigma^2}{2}, \sigma^2\right)$ represents log-normally distributed measurement error, independent and identically distributed for all t , with scale parameter $\sigma > 0$. In [Kreutz et al \(2007\)](#), this multiplicative log-normally distributed error model turns out to capture biological variability and experimental noise most adequately for observed concentrations which are non-negative. The parametrisation of the random variable $\varepsilon(t)$ ensures that $\mathbb{E}[\varepsilon(t)] = 1$ meaning that $\mathbb{E}[Y(t)] = \eta(t)$.

For both the exponential and the logistic growth model, we combine all possible unknown model and error parameters into the parameter vectors

$$\boldsymbol{\theta}^{(e)} = (\beta_1, \beta_2, x_1(0), x_2(0), \sigma)^T \in \mathbb{R}^2 \times \mathbb{R}_+^3 = \prod_{j=1}^5 \Theta_j^{(e)} = \Theta^{(e)},$$

and

$$\boldsymbol{\theta}^{(l)} = (\lambda_1, \lambda_2, K, x_1(0), x_2(0), \sigma)^T \in \mathbb{R}^2 \times \mathbb{R}_+^4 = \prod_{j=1}^6 \Theta_j^{(l)} = \Theta^{(l)},$$

respectively. The statistical methods described in the following can be applied for both models. For the remainder of this section, we, therefore, use $\boldsymbol{\theta} \in \prod_j^p \Theta_j = \Theta$ as a generic parameter vector with $p \in \mathbb{N}$ components, representing both $\boldsymbol{\theta}^{(e)}$ and $\boldsymbol{\theta}^{(l)}$. We let $\mathbf{y} = (y_1, \dots, y_n)$ denote a data set with n measurements taken at time points $0 \leq$

$t_1 \leq \dots \leq t_n$. We introduce maximum likelihood estimation to infer the components of $\boldsymbol{\theta}$ based on a data set \mathbf{y} . In addition, we introduce profile likelihoods to calculate confidence intervals and to investigate parameter identifiability. These methods are applied in Sections 4 and 5 to infer the model parameters for simulated scenarios as well as for knockout experiments in PDX models of acute leukaemia.

3.1 Parameter estimation

The measurements of the data set \mathbf{y} are assumed to be independent realisations of the random variable Y from Equation (7) at the respective time points. After log-transformation, we find that the difference

$$\log(Y(t)) - h(\mathbf{x}(t), \boldsymbol{\theta}) = \log(Y(t)) - \log\left(\frac{x_1(t)}{x_1(t) + x_2(t)}\right) + \frac{\sigma^2}{2} \sim \mathcal{N}(0, \sigma^2),$$

for $h(\mathbf{x}(t), \boldsymbol{\theta}) = \log(x_1(t)/(x_1(t) + x_2(t))) - \sigma^2/2$, is normally distributed. This property allows us to apply statistical methods based on the normal distribution. For the data set \mathbf{y} , the log-likelihood function reads

$$\ell(\mathbf{y}|\boldsymbol{\theta}) = \sum_{i=1}^n \log \phi(\log(y_i)|h(\mathbf{x}(t_i), \boldsymbol{\theta}), \sigma^2), \quad (8)$$

where $\phi(\log(y_i)|h(\mathbf{x}(t_i), \boldsymbol{\theta}), \sigma^2)$ is the density function of the normal distribution with mean $h(\mathbf{x}(t_i), \boldsymbol{\theta})$ and standard deviation σ . The maximum likelihood estimate of $\boldsymbol{\theta}$ is given by

$$\hat{\boldsymbol{\theta}} = \arg \max_{\boldsymbol{\theta} \in \Theta} \ell(\mathbf{y}|\boldsymbol{\theta}).$$

3.2 Profile likelihood

Since observations are subject to noise, parameters are estimated with uncertainty. To assess the precision of an estimate, we calculate confidence intervals for the components of $\boldsymbol{\theta}$ based on profile likelihoods. The profile likelihood of a parameter θ_j is defined by (Raue et al, 2009)

$$\text{PL}_j(q) = \max_{\{\boldsymbol{\theta}|\theta_j=q\}} \ell(\mathbf{y}|\boldsymbol{\theta}), \quad q \in \Theta_j.$$

To compute $\text{PL}_j(q)$, the log-likelihood is maximised with respect to all components θ_l , $l \neq j$, keeping $\theta_j = q$ fixed. By evaluating $\text{PL}_j(q)$ for a range of values q around the component $\hat{\theta}_j$ of the maximum likelihood estimate $\hat{\boldsymbol{\theta}}$, the shape of the likelihood along the axis of θ_j is explored. An approximate likelihood-based confidence interval for θ_j at confidence level $1 - \alpha$ is then given by

$$\text{CI}_{1-\alpha}^{\chi_1^2}(\theta_j) = \left\{ q \mid -2 \cdot \text{PL}_j(q) \leq -2 \cdot \ell(\mathbf{y}|\hat{\boldsymbol{\theta}}) + \Delta_{\alpha}^{\chi_1^2} \right\}, \quad (9)$$

where $\Delta_{\alpha}^{\chi_1^2}$ denotes the $(1 - \alpha)$ -quantile of the χ^2 -distribution with one degree of freedom (in short: χ_1^2 -distribution), for $\alpha \in (0, 1)$ (Raue et al, 2010). A confidence interval $\text{CI}_{1-\alpha}^{\chi_1^2}(\theta_j)$ consists of the union of disjoint intervals, if the negative profile likelihood intersects the confidence threshold $-\ell(\mathbf{y}|\hat{\boldsymbol{\theta}}) + 0.5 \cdot \Delta_{\alpha}^{\chi_1^2}$ more than twice.

Tönsing et al (2023) show that the type of confidence interval from Equation (9), assuming an asymptotic setting with the χ_1^2 -distribution, often inaccurately reflects parameter uncertainty for dynamic models in finite-sample cases. We investigate the appropriateness of this asymptotic assumption for both growth models in Section 5.1 for experimental data of gene modification experiments.

In the following, we show how the confidence intervals defined in (9) are used to check parameter identifiability. Moreover, in Section 4.2, we introduce an evaluation method of the gene modification experiments for the exponential growth model relying on the confidence interval of a growth parameter.

3.3 Parameter identifiability

Before we compute and interpret parameter estimates, we check whether the model parameters can be unambiguously identified. The literature distinguishes between two types of parameter identifiability: a parameter θ_j is called structurally identifiable if a unique maximum of $\ell(\mathbf{y}|\boldsymbol{\theta})$ exists with respect to θ_j . Otherwise, the parameter θ_j is structurally non-identifiable. In this case, $\text{PL}_j(q)$ is, in general, constant, which means that the model parametrisation is ambiguous in the sense that different parameter values yield the same model trajectories of $\mathbf{x}(t)$ or $\eta(t)$ (Raue et al, 2010). Structural non-identifiability can usually be resolved by a model reparametrisation or fixing parameters to certain values (Wieland et al, 2021). A more detailed discussion on structural identifiability is given in Anstett-Collin et al (2020) which further distinguishes between local and global identifiability.

Even if a parameter θ_j is structurally identifiable, insufficient data may still hamper to determine its value with finite confidence bounds. In this case, the negative profile likelihood $PL_j(q)$ only exceeds the confidence threshold in Equation (9) in one direction at most. Therefore, parameter θ_j is said to be practically identifiable if the confidence interval $CI_{1-\alpha}^{\chi_1^2}(\theta_j)$ is finite, for a confidence level $1 - \alpha$ (Raue et al, 2010). To make a practically non-identifiable but structurally identifiable parameter identifiable, the data quality or quantity must be increased to narrow its confidence interval (Wieland et al, 2021).

4 Evaluation of effect detection performance for simulated data

In a simulation study, we investigate whether incorporating domain-specific knowledge about the data generating process makes the analysis of time-resolved data more informative than a statistical test. We simulate data from a stochastic process relating to different growth-inhibiting scenarios of leukaemia cell populations. Sample sizes and effect sizes are motivated by the data from knockout experiments in PDX models used in our study. We represent the process by an exponential and logistic growth model and compare their detection performance with paired t -tests in various scenarios.

Before we introduce the evaluation methods and simulation scenarios, we check structural identifiability of the two growth models. In this section as well as in Section 5, we apply the `dMod` package in R to estimate their parameters and to calculate profile likelihood-based confidence intervals. For this purpose, we add an L_2 -constraint on the parameters to the objective function such that the trust region optimiser avoids selecting extreme parameter values of a possibly non-identifiable model. We remove the constraint for assessing identifiability and for computing confidence intervals as these concepts require data-based results (Kaschek et al, 2019; Riesle et al, 2023).

4.1 Structural identifiability of the growth models

We investigate structural identifiability of the parameters of both the exponential and the logistic growth model using profile likelihoods. For this analysis, we use simulated data of comparably large sample size. We compute one trajectory for each ODE model

for one concrete parameter setting using the simulation method from the **dMod** package. We extract the computed values for every integer time point between 0 and 50. We multiply each value with log-normally distributed random values to obtain realisations of the random variable Y from Equation (7). By this means, we simulate 20 observations for each time point yielding one data set for each growth model, each containing 1020 observations.

The exponential growth model exhibits the parameter vector $\boldsymbol{\theta}^{(e)} = (\beta_1, \beta_2, x_1(0), x_2(0), \sigma)^T$ and we set $\boldsymbol{\theta}^{(e)} = (0.1, 0.2, 10, 10, 0.2)^T$ for the data generation. Since $x_1(0)$, $x_2(0)$ and σ are assumed to be non-negative, we consider log-transforms of these components during numerical optimisation; this way, we can apply the trust region optimiser `trust` from **dMod** for performing unconstrained optimisation. The profile likelihoods of $\boldsymbol{\theta}^{(e)}$ reveal that all components except σ are structurally non-identifiable as the negative profile likelihoods exhibit no unique minimum (Figure 7, Appendix B). This finding is hardly surprising taking into account how the parameters are related within the closed-form expression of the observable function in Equation (6): the initial conditions are contained as a ratio and the growth parameters form the relative net growth of both populations. Therefore, we reparametrise the model with $\boldsymbol{\theta}^{(e)} = (\theta_1^{(e)}, \theta_2^{(e)}, \theta_3^{(e)})^T$ by setting

$$\theta_1^{(e)} = \beta_2 - \beta_1, \quad \theta_2^{(e)} = \frac{x_2(0)}{x_1(0)}, \quad \theta_3^{(e)} = \sigma,$$

thus decreasing the dimension of $\boldsymbol{\theta}^{(e)}$ from five to three while retaining the name of the overall parameter. Again, we log-transform $\theta_2^{(e)}$ and $\theta_3^{(e)}$ for numerical unconstrained optimization. All components of $\boldsymbol{\theta}^{(e)}$ turn out to be structurally identifiable (Figure 8, Appendix B).

For the logistic growth model and its parameter vector $\boldsymbol{\theta}^{(l)} = (\lambda_1, \lambda_2, K, x_1(0), x_2(0), \sigma)^T$, we set $\boldsymbol{\theta}^{(l)} = (0.1, 0.2, 1000, 10, 10, 0.2)^T$ for the data simulation. We log-transform the parameters K , $x_1(0)$, $x_2(0)$, and σ . The profile likelihoods of the components of $\boldsymbol{\theta}^{(l)}$ show that K , $x_1(0)$ and $x_2(0)$ are structurally non-identifiable (Figure 9, Appendix B). When we set $x_1(0) = 10$ to the true value of the data generation, we obtain a structurally identifiable model (Figure 10, Appendix B). However, if the growth parameters λ_1 and λ_2 are equal, e. g. $\lambda_1 = \lambda_2 = 0.1$, both parameters are structurally non-identifiable, even if $x_1(0)$ is fixed.

4.2 Evaluation methods

The parameters $\theta_1^{(e)} = \beta_2 - \beta_1$, $\theta_1^{(l)} = \lambda_1$ and $\theta_2^{(l)} = \lambda_2$ describe the growth behaviour of the two leukaemia cell populations within the exponential and the logistic growth model, respectively. Based on confidence intervals related to these parameters, we evaluate simulated experimental scenarios in Section 4.3.3 as well as real-world experiments in PDX models of acute leukaemia in Section 5.

The parameter $\theta_1^{(e)}$ of the exponential growth model reflects the net growth of the modified Population 1 in relation to Population 2. If the confidence interval $\text{CI}_{1-\alpha}^{\chi_1^2}(\theta_1^{(e)})$, for $\alpha \in (0, 1)$, excludes zero, we deduce that the growth behaviour of Population 1 differs significantly from that of Population 2. This is equivalent to a two-tailed significance test with null hypothesis $H_0 : \theta_1^{(e)} = 0$ and alternative hypothesis $H_1 : \theta_1^{(e)} \neq 0$ at significance level α . We find in Section 5.1 that the approximate confidence interval $\text{CI}_{1-\alpha}^{\chi_1^2}(\theta_1^{(e)})$, as defined in Equation (9), tends to underestimate parameter uncertainty for knockout experiments in PDX models using quantiles of the χ_1^2 -distribution. For a confidence level of 95 %, we therefore calculate confidence intervals $\text{CI}_{0.95}^{\text{Cant}}(\theta_1^{(e)})$ using the adapted threshold $\Delta_{0.05}^{\text{Cant}} = 7.16$ in addition to using the quantile $\Delta_{0.05}^{\chi_1^2} = 3.84$ of the χ_1^2 -distribution, as suggested in Tönsing et al (2023).

For the logistic growth model, the parameters $\theta_1^{(l)}$ and $\theta_2^{(l)}$ describe the net growth of Population 1 and Population 2, respectively. We again deduce that the growth behaviour of Population 1 differs significantly from that of Population 2 if a confidence interval for $\theta_2^{(l)} - \theta_1^{(l)}$ excludes zero. We compute such a confidence interval $\text{CI}_{1-\alpha}^{\text{boot}}(\theta_2^{(l)} - \theta_1^{(l)})$ using nonparametric bootstrap. Within the bootstrap, we sample from an underlying data set maintaining the original design. For example, for a data set with a total of 16 observations and two different output measurement times, t_1 and t_2 , of four observations each, we sample with replacement four observations from each t_1 and t_2 and eight input measurements from day 0. We re-estimate $\hat{\theta}_1^{(l)}$ and $\hat{\theta}_2^{(l)}$ for several of these bootstrap samples and derive a $(1 - \alpha)$ -confidence interval for $\theta_2^{(l)} - \theta_1^{(l)}$ based on the bootstrap estimates $\hat{\theta}_2^{(l)} - \hat{\theta}_1^{(l)}$. Checking whether the resulting confidence interval excludes zero is equivalent to a significance test with hypotheses $H_0 : \theta_2^{(l)} - \theta_1^{(l)} = 0$ vs. $H_1 : \theta_2^{(l)} - \theta_1^{(l)} \neq 0$ for significance level α .

The standard evaluation approach applies paired t -tests to compare measurements from only two different time points per experiment. The test assesses whether the mean difference between the paired input and output measurements differs significantly from

zero. The test statistic is given by

$$\tau = \frac{\frac{1}{m} \sum_{j=1}^m (y_j(0) - y_j(t_{\text{out}}))}{\frac{\sigma_D}{\sqrt{m}}},$$

where $y_j(0)$ and $y_j(t_{\text{out}})$ denote the input measurement from day 0 and output measurement from day t_{out} of mouse j , respectively, and σ_D denotes the empirical standard deviation of the differences between all m mice considered. The corresponding hypotheses are $H_0 : \tau = 0$ vs. $H_1 : \tau \neq 0$ for significance level α . We conduct these t -tests without multiple testing correction, as the focus of our analysis is to individually compare the method of t -tests with model-based evaluations.

Although we are mainly interested in assessing whether a gene modification causes a cell population growth-inhibiting effect, i. e. $H_1 : \theta_1^{(e)} > 0$, $H_1 : \theta_2^{(l)} - \theta_1^{(l)} > 0$, or $H_1 : \tau > 0$, we relate our evaluations to two-tailed significance tests; this is consistent with the standard procedure to analyse the experiments with two-tailed paired t -tests (e. g. [Ghalandary et al, 2023](#)). We however retain to refer to the aim to recognise possible population growth-inhibiting effects.

4.3 Simulation study: evaluation of detection methods

We evaluate the detection performance of the growth models with paired t -tests for simulated experimental scenarios. An appropriate detection method recognises present effects reliably, and if there are no effects in the data generating process, none should be recognised.

4.3.1 Data simulation with Gillespie's algorithm

We generate data sets mimicking scenarios with different effect and sample sizes with Gillespie's algorithm ([Gillespie, 1976, 1977](#)) using the R package `GillespieSSA` (Version 0.6.2, [Pineda-Krch, 2008](#)). Gillespie's algorithm simulates exact trajectories of a Markov jump process (MJP), i. e. a continuous-time Markov process with discrete states. Compared to a deterministic ODE representation that we have considered so far, an MJP represents the temporal sequence of biochemical reactions stochastically. It can be shown that the length of time intervals between two consecutive reactions is exponentially distributed for an MJP, which is utilised by Gillespie's algorithm. Due to the discrete nature and stochasticity of biological systems, MJPs and Gillespie's algorithm are commonly used to describe and simulate reaction networks, such

as cell reactions in our case (Wilkinson, 2019). However, the likelihood of an MJP is, in general, intractable which makes statistical inference challenging. Therefore, an ODE approximation is often used to represent reaction networks and to infer model parameters based on data.

Since Gillespie's original direct method is computationally intensive for large cell numbers, we apply the approximate optimised tau-leaping method (Cao et al, 2006) implemented in GillespieSSA to simulate trajectories of the state variable $\mathbf{x}(t)$. For the data simulation, we assume that a leukaemia cell of both populations can perform one out of two reactions at any time, it can either proliferate or die. These two reactions occur with rates r_1 and r_2 for Population 1, and with r_3 and r_4 for Population 2. We consider four scenarios with different parameter settings mimicking experiments with no gene modification effect, and with a small, medium and strong modification effect. We impose that a gene modification only affects the cell death rate r_2 of Population 1, while the proliferation activity of both populations and cell death of Population 2 remain unaffected. Therefore, only r_2 varies across the scenarios, and the chosen values of the rate parameters are listed in Table 1. For all scenarios, we set $x_1(0) = x_2(0) = 5 \cdot 10^4$ and, to generate realisations of Y from Equation (7), we set $\sigma = 0.2$.

Table 1: Parameter values of the reaction rates to simulate four experimental scenarios with Gillespie's algorithm, where we further set $x_1(0) = x_2(0) = 5 \cdot 10^4$ and $\sigma = 0.2$ for all scenarios

Scenario	r_1	r_2	r_3	r_4
no effect	0.2	0.11	0.2	0.11
weak effect	0.2	0.13	0.2	0.11
medium effect	0.2	0.15	0.2	0.11
strong effect	0.2	0.21	0.2	0.11

For each scenario, we simulate 100 data sets each mimicking a real experiment designed with two output measurement times, in this case day 14 and day 40. As each combination of one input (from day 0) and one output measurement (from day 14 or 40) corresponds to one mouse in knockout experiments in PDX models, we generate one Gillespie trajectory for each combination. We consider four sample size settings. In the first setting, we assume that two fictitious mice are sacrificed and measured after 14 days and two more after 40 days, resulting in an overall sample size of eight measurements, i. e. four output measurements together with four input measurements from day 0. In the remaining three settings, we consider data sets with sample sizes

of 16, 32 and 64, where four, eight and sixteen fictitious mice each are measured on day 14 and 40. In total, we thus simulate 1600 data sets.

4.3.2 Practical identifiability

We analyse the simulated experiments, aiming to detect modification effects at significance level $\alpha = 0.05$. We calculate profile-likelihood based confidence intervals for $\theta_1^{(e)}$ of the exponential growth model using the quantile $\Delta_{0.05}^{\chi_1^2}$ and the adapted threshold $\Delta_{0.05}^{\text{Cant}}$, as explained in Section 5.1. Irrespective of the threshold for the confidence intervals, the profile likelihoods of $\theta_2^{(e)}$ and $\theta_3^{(e)}$ reveal that these parameters are practically identifiable for each of the 1600 data sets. Parameter $\theta_1^{(e)}$ is practically identifiable for all except one of these data sets.

For the estimation of $\boldsymbol{\theta}^{(l)}$ of the logistic growth model, we set $\theta_4^{(l)} = x_1(0) = 5 \cdot 10^4$ to obtain a structurally identifiable model. We additionally fix the carrying capacity and set $\theta_3^{(l)} = K = 10^9$ to facilitate model estimation. We use the quantile $\Delta_{0.05}^{\chi_1^2}$ to calculate approximate confidence intervals according to Equation (9), justified by the analysis in Section 5.1. The confidence intervals show that the parameters $\theta_5^{(l)} = x_2(0)$ and $\theta_6^{(l)} = \sigma$ are practically identifiable for all but one of the 1600 data sets each. As proliferation and cell death rates for both populations are equal for the scenario of no modification effect, the growth parameters $\theta_1^{(l)} = \lambda_1$ and $\theta_2^{(l)} = \lambda_2$ are practically non-identifiable (except for five data sets for numerical reasons), as both parameters are structurally non-identifiable for $\theta_1^{(l)} = \theta_2^{(l)}$. For the weak modification effect and a sample size of 8 measurements, $\theta_1^{(l)}$ and $\theta_2^{(l)}$ are practically identifiable for around 35 of the 100 data sets. The stronger the modification effect or the larger the sample size, the more frequently the two growth parameters can be practically identified. For a medium or strong modification effect, both parameters are practically identifiable for at least 59 of the corresponding 100 data sets.

4.3.3 Exponential growth model reveals ground truth most reliably

Figure 5 displays the proportions of detected effects for all evaluation methods, simulated modification scenarios and sample sizes. An overview of the single detection results is shown in Figure 11 in Appendix B for each simulated data set and all evaluation methods. An evaluation method performs reliably if it does not recognise a modification in the first scenario but detects the assumed growth-inhibiting effects in all other scenarios.

In the first scenario without any imposed modification, the logistic growth model shows the highest number of allegedly identified growth-inhibiting effects among the considered evaluation methods for sample sizes of 8 and 16 measurements. Around half of these effects are declared to be growth-enhancing, i. e. $\text{CI}_{0.95}^{\text{boot}}(\theta_2^{(l)} - \theta_1^{(l)}) \subset \mathbb{R}_+$. These proportions are represented by the dashed parts of the bars in Figure 5. For sample sizes of 32 and 64 measurements, the logistic growth model hardly flags any significant effect. This is similar to the exponential growth model with adapted threshold $\Delta_{0.05}^{\text{Cant}}$, which shows the least identified effects among the considered methods for all sample size settings and the unmodified scenario. Due to the more conservative construction of the confidence interval $\text{CI}_{0.95}^{\text{Cant}}(\theta_1^{(e)})$, the set of cases with detected effects according to the exponential growth model with adapted threshold $\Delta_{0.05}^{\text{Cant}}$ is always a subset of the cases classified as growth-inhibiting according to the exponential growth model with quantile $\Delta_{0.05}^{\chi_1^2}$. Aside from this, several of the allegedly identified effects overlap across the different evaluation methods for the first three sample sizes. For the largest sample size, $n = 64$, however, all methods except the paired t -tests for day 14 measurements agree on the same set of alleged effects (cf. Figure 11, Appendix B).

If there is a weak modification effect present in the data generation, the exponential growth model with quantile $\Delta_{0.05}^{\chi_1^2}$ performs best in detecting modification effects (cf. Figure 5). We note that this method captures nearly all effects detected by the other methods for sample sizes 8 and 16. For larger sample sizes, this comparison becomes less relevant, as all methods except the paired t -tests for day 14 measurements perform similarly well (cf. Figure 11, Appendix B). It is also worth noting that in a no-effect scenario with $n = 8$, this is the only setting in which the logistic growth model identifies effects more reliably than the exponential growth model with adapted threshold $\Delta_{0.05}^{\text{Cant}}$ and than the two paired t -tests.

Regarding the sample size, however, it appears disadvantageous for the t -tests to compare their detection performance with the growth model-based approaches from the same indicated sample size, i. e. comparing the corresponding bars within the same row in Figure 5. That is because of the special design of the simulated datasets, where the output measurements are split into those for day 14 and those for day 40. The t -tests are computed based on only one output measurement time each, whereas the model-based methods take into account measurements of both time points. Thus, the growth models rely on sample sizes twice as large as for the t -tests. This represents one of the strengths associated with our model-based approaches: they can handle

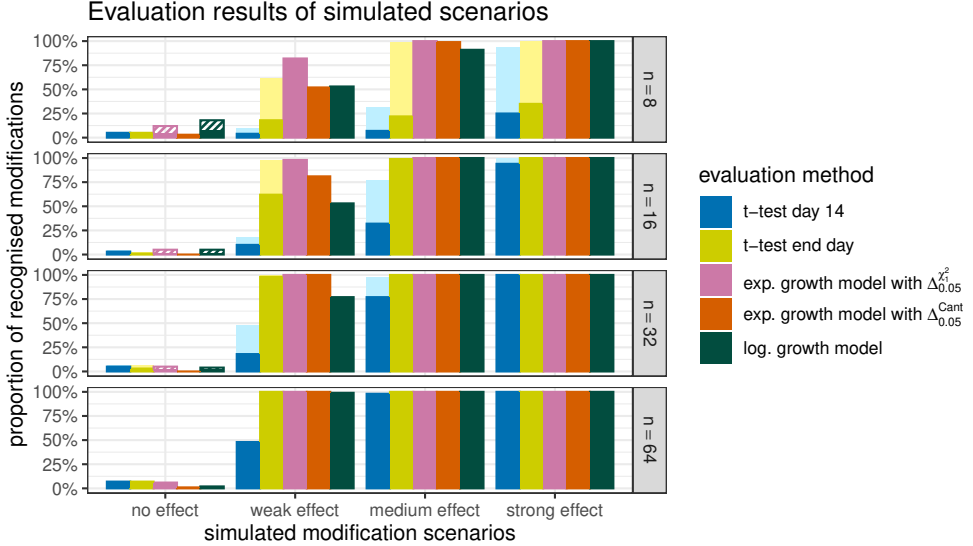


Fig. 5: Detection results for simulated data via five evaluation methods: paired t -tests for two different end days, the exponential growth model (once with quantile $\Delta_{0.05}^{X_1^2} = 3.84$, once with adapted threshold $\Delta_{0.05}^{\text{Cant}} = 7.16$ for profile likelihood-based 95 % confidence intervals of $\theta_1^{(e)}$), and the logistic growth model based on 95 % bootstrapping confidence intervals for $\theta_2^{(l)} - \theta_1^{(l)}$. The data stems from four simulated scenarios and four sample size settings. Dashed parts represent the proportion of confidence intervals for the corresponding evaluation quantity which are a subset of \mathbb{R}_+ , indicating a growth-enhancing rather than growth-inhibiting effect. Light blue and light yellow bars represent the numbers of detected modification effects of a corresponding scenario for the next larger sample size for paired t -tests of day 14 measurements and endpoint measurements, respectively. Figure 11 in Appendix B provides a detailed visualisation of detection results per dataset, revealing individual (dis-)agreement between evaluation methods

measurements taken at different points in time, as is the case in the motivating dataset of our study. However, for an alternative comparison, we also include light shaded bars in Figure 5 showing the t -test results of the next larger sample size. This way, the bars of growth model-based evaluations for a sample size of, e.g., $n = 8$ can directly be compared with the bars of the t -tests for $n = 16$. This consideration particularly plays a role for the sample sizes $n = 8$ and $n = 16$. Accounting for that, the t -tests for day 40 measurements recognise weak effects more reliably as the exponential growth model with adapted threshold $\Delta_{0.05}^{\text{Cant}}$ and as the logistic growth model. For larger sample sizes, this consideration becomes negligible.

In the medium and strong modification scenario, the exponential and logistic growth models perform equally well in recognising almost all modification effects for all sample size settings. For sample size $n = 8$ and the split data sets, both t -tests identify less than half of the modifications of the two scenarios (cf. Figure 5). Moreover, the effects identified by the two t -tests overlap only partially (cf. Figure 11, Appendix B).

However, considering the t -test results for $n = 16$ shows that especially the t -tests for day 40 measurements recognise all modifications just like the exponential growth model. For larger sample sizes, all considered approaches identify modifications equally well.

All in all, the exponential growth model with quantile $\Delta_{0.05}^{\chi_1^2}$ detects existing modification effects in the data the most. The more conservative approach for the exponential growth model with adapted threshold $\Delta_{0.05}^{\text{Cant}}$ detects nearly as many modifications as paired t -tests for day 40 measurements, if the actual underlying sample sizes agree. The logistic growth model performs worse than the exponential growth model and than the paired t -test for day 40 measurements in the simulation study. Only paired t -tests for day 14 measurements recognise fewer existing modification effects in the data. The exponential growth model with adapted threshold $\Delta_{0.05}^{\text{Cant}}$ detects the fewest modifications if none were imposed in the data generation.

Even though a logistic growth model might, in general, reflect growth of populations more realistically than exponential growth, it seems to be too complex in our application. The unknown model parameters, especially the growth parameters $\theta_1^{(l)}$ and $\theta_2^{(l)}$ of the two-dimensional ODE system, are challenging to statistically infer based on the one-dimensional observable and on the small sample sizes. Even if $\theta_1^{(l)} \neq \theta_2^{(l)}$ and if both growth parameters are practically identifiable, their confidence intervals tend to be relatively broad and the profile likelihoods are flat around the maximum likelihood estimate. Extreme parameter estimates are mainly prevented by the L_2 -constraint added to the likelihood. The L_2 -constraint is also utilised within the bootstrap for the confidence interval $\text{CI}_{0.95}^{\text{boot}}(\theta_2^{(l)} - \theta_1^{(l)})$ such that the whole uncertainty about estimating $\theta_2^{(l)} - \theta_1^{(l)}$ might not be represented by the resulting bootstrap intervals. For this reason, the number of recognised modification effects by the logistic growth model might be affected by these circumstances.

Nonetheless, we also need to note that the framework for Gillespie's algorithm generates a Markov jump process, whose deterministic approximation, i. e. the so-called reaction rate equation, equals the two-dimensional exponential growth model. Thus, the data generation favours the exponential growth model over logistic growth in terms of parameter estimation.

5 Analysis of gene knockout trials in PDX models

In preclinical trials, PDX models of acute leukaemia are genetically modified to explore therapeutic targets. We evaluate measurements of a series of gene knockout experiments for five acute lymphocytic leukaemia (ALL) and two acute myeloid leukaemia (AML) PDX models. For each of these samples, up to seven genes were knocked out and the modified cells were injected into mice. The considered seven genes had turned out to be most promising for reducing cell population growth in a CRISPR-Cas9 knockout screening approach with around 100 genes. This results in a total of 44 single knockout experiments. We anonymise the gene names in this work and each gene is assigned a unique identifier, a number between 1 and 7.

Six of the seven genes were pairwise combined for engraftment for some leukaemia samples such that a mouse was endowed with in total three cell populations, i. e. two modified populations and the control population, to reduce the number of mice used. The specific gene pairs are gene 1 and gene 4, gene 2 and gene 3, and gene 5 and gene 7 (cf. Table 3, Appendix A). This circumstance has no effect on the application of the exponential growth model, as the cell populations behave independently of each other within this model. Within the logistic growth model, however, the different populations compete with each other for the limited capacity in the bone marrow. Following a comparison of the data characteristics, we still follow the two-dimensional logistic growth model rather than employing a model with three state variables x_1 , x_2 , and x_3 . This procedure serves the goal of showcasing our principle to experimental data. Consequently, we treat all measurements of the 44 gene knockout experiments as if they were taken from PDX models endowed with two cell populations.

To perform a specific CRISPR-Cas9-based gene knockout, up to three different sgRNAs were used per knockout experiment. For each experiment, mice were sacrificed on up to two different days in the course of the experiments. One of these days is around day 14 after injection of the cells and the second is a later day that is at an advanced stage of leukaemia, which is sample-specific. On these days, cell numbers in the bone marrow of mice were measured by flow cytometry. As the corresponding input measurements are available from day 0, up to three measurement times are available per experiment to investigate growth-inhibiting effects. Information about the individual experiments is collected in Table 3 in Appendix A.

Table 3 in Appendix A also contains p -values of paired t -tests comparing measurements from an early time point (around day 14) and from a variable endpoint day with the corresponding input measurements from day 0 at a confidence level $1 - \alpha = 0.95$. For the variable endpoint measurements, the two-tailed paired t -tests detect significant growth-inhibiting effects for the modified cell populations in 40 of 44 experiments (cf. Table 2). For the measurements around day 14, the t -tests reveal significant growth-inhibiting effects for the cell populations in 33 of 38 experiments (six experiments contain less than two measurements for a day around day 14, so the paired t -test is not applicable in these cases).

In the following, we statistically infer the parameters of the exponential and the logistic growth model for the knockout experiments. To facilitate estimation, we set 14 measurements with a value smaller than 0.0001 equal to this threshold value, as our model assumes strictly positive observations according to Equation (7). We fix the parameter $\theta_4^{(l)} = x_1(0)$ to the absolute input value of the single experiments to make the logistic growth model structurally identifiable for $\theta_1^{(l)} \neq \theta_2^{(l)}$ (cf. Table 3, Appendix A). Nevertheless, the property $\theta_1^{(l)} = \theta_2^{(l)}$ might be true for a knockout data set, which would be a data-driven characteristic. However, in general terms, this property has probability zero if probability densities are assigned to the \mathbb{R} -valued parameters $\theta_1^{(l)}$ and $\theta_2^{(l)}$. As long as the parameters are unequal, regardless of how small their difference is, they are structurally identifiable. Moreover, we fix the carrying capacity $\theta_3^{(l)} = K$ of the logistic growth model to the maximum cell number that has ever been measured for the single leukaemia samples to further facilitate parameter estimation (cf. Table 3, Appendix A).

Before we discuss estimation results and evaluate the knockout experiments, we verify the asymptotic χ_1^2 -distribution assumption in Equation (9) for profile likelihood-based confidence intervals of components of the parameter vectors $\boldsymbol{\theta}^{(e)}$ and $\boldsymbol{\theta}^{(l)}$.

5.1 Verification of the approximate χ_1^2 -distribution assumption for confidence intervals

The 44 knockout data sets each contain a maximum of 22 observations. To ensure valid confidence intervals for these finite-sample cases, we check whether it is appropriate to assume the asymptotic χ_1^2 -distribution assumption for confidence intervals of the components of $\boldsymbol{\theta}^{(e)}$ and $\boldsymbol{\theta}^{(l)}$ in Equation (9). We first estimate $\boldsymbol{\theta}^{(e)}$ and $\boldsymbol{\theta}^{(l)}$ for each of the 44 knockout data sets, including all measurements of the different sgRNAs used in

each experiment. [Tönsing et al \(2023\)](#) present a bootstrapping approach to calculate empirical likelihood ratios of the parameters whose cumulative distribution function (ECDF) is compared to the theoretical cumulative distribution function (CDF) of the χ_1^2 -distribution. This comparison can be visualised by probability-probability plots (pp-plots), which display the empirical distribution against the theoretical distribution ([Tönsing et al, 2023](#)) . In an analysis of 19 benchmark ODE models from the systems biology literature, they find that the approximate distribution assumption for empirical likelihood ratios of only 52 % of the parameters is appropriate. In these cases, the pp-plot graph either lies in the perfect consensus region around the diagonal or in the upper left triangle of the pp-plot. The latter cases are classified as conservative as for those the ECDF is larger than the CDF which means that profile likelihood-based confidence intervals tend to be too large. If the ECDF, however, is considerably smaller for some values than the CDF, [Tönsing et al \(2023\)](#) distinguish again between two cases: if the pp-plot graph lies completely in the lower right triangle, the graph is classified as anti-conservative. If the pp-plot graph crosses both regions around the diagonal, the graph is termed alternating. In both cases, confidence intervals might be too small for certain confidence levels.

The bootstrapping results of the exponential growth model for the experimental data of gene knockouts are even more severe than those from the literature. The pp-plot graphs of only about 37 % of all parameters of $\theta^{(e)}$ for the 44 data sets are assigned to the perfect consensus region or the conservative class. All other graphs are classified as anti-conservative. In particular, the pp-plot graphs of the error parameter $\theta_3^{(e)}$ are assigned to the anti-conservative class for 37 experiments. The pp-plot graphs of the growth parameter $\theta_1^{(e)}$ are anti-conservative or alternating for 18 experiments (Figure 12, Appendix B). If we examine the pp-plot graphs for a confidence level of $1 - \alpha = 0.95$, about 46 % of all graphs are classified as anti-conservative at this level. In these cases, a confidence interval based on Equation (9) would be too small with the quantile $\Delta_{0.05}^{\chi_1^2} = 3.84$. In the following, we thus adopt the suggestion from [Tönsing et al \(2023\)](#) to use an adapted threshold for profile likelihood-based 95 % confidence intervals for $\theta^{(e)}$. The threshold $\Delta_{0.05}^{\text{Cant}} = 7.16$ based on Cantelli's inequality yields larger confidence intervals, compared to the asymptotic threshold, accounting for a potential underestimation of parameter uncertainty. We denote such a confidence interval with adapted threshold by $\text{CI}_{0.95}^{\text{Cant}}(\theta_j^{(e)})$, for $j = 1, 2, 3$.

For the logistic growth model, we apply the bootstrapping approach to the components of $\boldsymbol{\theta}^{(l)}$, while keeping $\theta_3^{(l)}$ and $\theta_4^{(l)}$ fixed. We find that the pp-plot graphs of the growth parameters $\theta_1^{(l)}$ and $\theta_2^{(l)}$ are assigned to the perfect consensus region or the conservative class for 33 and 31 experiments, respectively. The pp-plot graphs of $\theta_5^{(l)}$ and $\theta_6^{(l)}$ are classified as anti-conservative for 28 and for all 44 experiments, respectively (cf. Figure 13, Appendix B). The classifications are almost identical if we examine the pp-plot graphs at a 95 % confidence level. According to these results, we stick to the asymptotic setting in Equation (9) for the logistic growth model, since we focus on the analysis of the experiments and are mainly interested in inferring $\theta_1^{(l)}$ and $\theta_2^{(l)}$. We therefore use the quantile $\Delta_{0.05}^{\chi_1^2} = 3.84$ of the χ_1^2 -distribution to compute confidence intervals for components of $\boldsymbol{\theta}^{(l)}$.

5.2 Practical identifiability and effect detection

It is reasonable to assume that the mice are heterogeneous and that they react differently to a specific gene knockout. To check this behaviour, we estimate a single exponential growth model for each pair of an input and output measurement (350 in total) which was involved in one of the 44 knockout experiments. We evaluate the knockout effects based on $\text{CI}_{0.95}^{\text{Cant}}(\theta_1^{(e)})$ for each pair and compare the evaluations among the pairs used for a specific knockout experiment. The parameters $\theta_1^{(e)}$ and $\theta_2^{(e)}$ are practically identifiable for each pair. However, the maximum likelihood estimation of the error parameter $\theta_3^{(e)}$ fails for each estimation, which is not surprising given that they are only based on two observations each. We find that the confidence intervals $\text{CI}_{0.95}^{\text{Cant}}(\theta_1^{(e)})$ for the pairs subject to the same gene knockout are either a subset of \mathbb{R}_+ or overlap zero. For no knockout, one confidence interval is a subset of \mathbb{R}_+ and a different one is a subset of \mathbb{R}_- . Thus, the directions of the evaluations coincide among the pairs of each knockout experiment. We, therefore, pool all observations related to different sgRNAs of a knockout experiment for model estimations without accounting for individual specific effects, such as mixed effects.

5.2.1 Practical identifiability

The confidence intervals $\text{CI}_{0.95}^{\text{Cant}}(\theta_j^{(e)})$ of the exponential growth model reveal that $\theta_1^{(e)}$ is practically identifiable for 33 experiments and $\theta_2^{(e)}$ for 29 experiments, whereas $\theta_3^{(e)}$ turns out to be practically identifiable for all 44 experiments (cf. Table 4). The

confidence intervals of the components of $\boldsymbol{\theta}^{(l)}$, in contrast, show fewer practically identifiable parameters: the parameters $\theta_1^{(l)} = \lambda_1$, $\theta_2^{(l)} = \lambda_2$ and $\theta_5^{(l)} = x_2(0)$ are practically identifiable for 26, 11 and 27 experiments, respectively. The parameter $\theta_6^{(l)} = \sigma$ is again practically identifiable for all 44 experiments (cf. Table 5). The relation of the practical identifiability status of the components of $\boldsymbol{\theta}^{(e)}$ and $\boldsymbol{\theta}^{(l)}$ and the classification of their pp-plot graph is consistent with the results from [Tönsing et al \(2023\)](#). They find that the pp-plot graphs of practically non-identifiable parameters are often assigned to the conservative class, whereas error parameters, as σ in our case, are often practically identifiable, but their pp-plot graphs are classified as anti-conservative.

5.2.2 Detected effects

For the exponential growth model, we assess cell population growth-inhibiting effects of gene knockouts based on the confidence interval $\text{CI}_{0.95}^{\text{Cant}}(\theta_1^{(e)})$, as introduced in Section 4.2. The confidence interval excludes zero for 31 experiments (cf. Table 2). In 30 of these experiments, the confidence interval is a subset of the positive real line, and we deduce that the specific gene knockout inhibits the growth of cell Population 1. For one experiment (AML-388 6), the interval is a subset of the negative real line, which would mean that the gene knockout had a growth-boosting effect. This is rather unlikely from a biological perspective and could be due to the fact that the estimation result for this experiment is only based on four measurements. All 30 significant growth-inhibiting experiments are also significant according to two-tailed paired *t*-tests for the variable endpoint measurements (cf. Figure 14, Appendix B). Applying the asymptotic threshold $\Delta_{0.05}^{x_1^2} = 3.84$ for profile likelihood-based confidence intervals would have revealed 40 significant knockout effects, including 37 *t*-test-based significant results for the variable endpoint measurements. Both methods flag only four experiments as non-growth-altering; however, they coincide in only one of these four cases (cf. Figure 14, Appendix B).

To evaluate the experiments based on the logistic growth model, we again compute confidence intervals $\text{CI}_{0.95}^{\text{boot}}(\theta_2^{(l)} - \theta_1^{(l)})$ applying the nonparametric bootstrap described in Section 4.2. We apply the bootstrap to the 38 experiments with a sample size of at least eight measurements (cf. Table 3, Appendix A), for which we can generate a sufficient number of bootstrap samples. The confidence interval excludes zero for 37 experiments, for which we deduce a significant growth-inhibiting effect based on the

logistic growth model (cf. Table 2). All these 37 experiments are among the 40 experiments which are significantly growth-inhibiting according to the paired t -tests for endpoint measurements (cf. Figure 14, Appendix B). Moreover, 28 (34) of these 37 experiments are among the 31 (40) significant knockouts recognised by the exponential growth model with threshold $\Delta_{0.05}^{\text{Cant}}$ (with quantile $\Delta_{0.05}^{\chi^2_1}$).

However, the same technical issues of estimating the logistic growth model occur for knockout experiments in PDX models as described for the simulation study in Section 4.3.3: the profile likelihoods of $\theta_1^{(l)}$ and $\theta_2^{(l)}$ are flat around the maximum likelihood estimate for several of the experiments for which the two parameters are practically non-identifiable. Again, an L_2 -constraint on the likelihood prevents extreme parameter estimates which might distort the bootstrap confidence intervals and thus the evaluation of the experiments based on logistic growth.

Table 2: Results for knockout experiments in PDX models: for each detection method, we list the number of considered experiments, the number of recognised significant gene knockout effects, and the number of recognised significant knockout effects that are growth-enhancing, i.e. for which the confidence interval of the corresponding evaluation method is a subset of \mathbb{R}_+ . Figure 14 in Appendix B provides a detailed visualisation of detection results per dataset, revealing individual (dis-)agreement between evaluation methods

Detection method	Considered experiments	Significant experiments	Of which growth-enhancing
t -test day 14	38	33	-
t -test end day	44	40	-
exp. growth model, $\Delta_{0.05}^{\chi^2_1}$	44	40	1
exp. growth model, $\Delta_{0.05}^{\text{Cant}}$	44	31	1
log. growth model	38	37	0

So far, we have combined the measurements for up to three different sgRNAs used for a specific knockout to estimate one exponential or logistic growth model. The number of used sgRNAs per knockout experiment are collected in Table 3 in Appendix A. Even though the most suitable sgRNAs were selected to knock out a gene, the chosen sgRNAs might differ in their knockout efficacy, as it could be the case for the ALL-199 2 experiment (Figure 6). To evaluate the knockouts for each considered sgRNA separately, we re-estimate the exponential growth model for each sgRNA used for a knockout for which more than one sgRNAs were used in total. Again, we exclude the experiments where an sgRNA was only applied to one mouse and thus only two observations were obtained. Hence, we consider a total of 113 data sets for 38 knockouts, with sample sizes ranging from four to eight measurements. Parameter $\theta_1^{(e)}$ is practically identifiable for 74 of these data sets. For 65 of the estimated models,

we find $\text{CI}_{0.95}^{\text{Cant}}(\theta_1^{(e)}) \subset \mathbb{R}_+$ and we deduce significant cell population growth-inhibiting effects for these knockouts and the single sgRNAs. Comparing the single evaluations for all sgRNAs used with respect to a specific knockout, we find that the significance of sgRNA sub-effects varies for 21 of the 38 knockouts: for these, the confidence interval $\text{CI}_{0.95}^{\text{Cant}}(\theta_1^{(e)})$ is a subset of the positive real line for at least one sgRNA and for at least one other sgRNA, the interval overlaps zero. As far as hypothesis tests are concerned, we can apply a paired t -test for the endpoint measurements to only 61 of the 113 data sets, as these data sets contain endpoint measurements of more than one mouse. In 45 of these cases, the t -tests for endpoint measurements provide a significant effect of gene knockout. All results for the separated sgRNA analysis are summarised in Table 6. As most of the separated estimations are based on data sets with less than eight observations, nonparametric bootstrap confidence intervals $\text{CI}_{0.95}^{\text{boot}}(\theta_2^{(l)} - \theta_1^{(l)})$ are inappropriate to compute for these small sample sizes. Together with the more challenging parameter estimation of the logistic growth model, we therefore refrain from a separated sgRNA analysis with the logistic growth model.

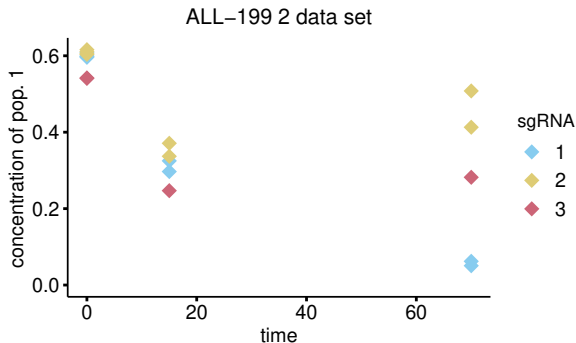


Fig. 6: Measurements of the ALL-199 2 experiment, for which three different sgRNAs were used that might have different knockout efficacy

6 Discussion and conclusion

We investigate whether incorporating mechanistic knowledge makes the detection of differences between underlying processes more reliable than a statistical test. We relate our analysis to gene knockouts in PDX samples of acute leukaemia as part of preclinical research. To describe the growth of leukaemia cell populations and to detect cell growth-inhibiting effects, we apply an exponential and a logistic growth model. We compare their detection performance with paired t -tests, which are often applied as standard, in several ways.

When applied to real data, we can observe that different detection methods lead to different results. However, in the absence of ground truth, this comparison does not yet allow us to determine which method is more reliable. In addition, the performance directly depends on the sample sizes. For that reason, we conduct a simulation study to compare the growth models with *t*-tests for analysing time-resolved data of a stochastic process related to gene modification experiments. Even though exponential growth is less suitable for describing and predicting population growth over a longer time period, our simulation study reveals that the exponential growth model performs well in evaluating the considered type of data sets. The model is less complex than the logistic growth model in terms of the number of parameters. Its parameters are easier to estimate and can be unambiguously identified more frequently. As a result, it adequately describes the course of the cell populations over the finite experimental time horizon and is suitable for experimental evaluation.

The logistic growth model turns out to be too complex for the considered data type. Since the profile likelihoods of $\theta_1^{(l)}$ and $\theta_2^{(l)}$ are often flat around the estimates, only an L_2 -constraint on the likelihood prevents extreme parameter estimates. This adaptation might explain the relatively high number of recognised modifications, both in the simulation study and for the experiments performed in PDX models, which needs to be taken into account when interpreting the evaluation results.

The evaluation results of the paired *t*-tests for the variable endpoint measurements can compete with the exponential growth model in the simulation study, provided that the sample size is sufficiently large and effects are present in the data-generating process: in that case, the *t*-test recognises approximately as many effects as the exponential growth model with adapted threshold $\Delta_{0.05}^{\text{Cant}}$. The *t*-test benefits from the allocation of the output measurements to a maximum of two measurement days. Thus, a paired *t*-test for late measurement times is an alternative to model-based approaches, particularly if growth-inhibiting effects are present. These effects, however, are typically unknown for PDX experiments. Moreover, the possibility of combining measurements into a single sample for the *t*-tests depends on the experimental conditions, which typically cannot be influenced at the time of data analysis. This represents a strength of the model-based methods.

For the knockout experiments in PDX models, the key comparison is between the exponential growth model with quantile $\Delta_{0.05}^{\chi^2_1}$, the version using the adapted threshold $\Delta_{0.05}^{\text{Cant}}$, and the paired *t*-test for the endpoint measurements: the first method most

reliably detects existing effects in the simulation study, the second is most effective at not flagging non-existing ones, and the third represents the established approach in practice. The framework of the knockout experiments aligns with the first two sample size settings of the simulation study ($n \in \{8, 16\}$), as the knockout experiments include at most $n = 22$ measurements. The conservative confidence intervals $\text{CI}_{0.95}^{\text{Cant}}(\theta_1^{(e)})$ for the knockout experiments suggest that the range of assumed effect sizes considered in the simulation study (from “none” to “strong”) represents a realistic assumption for the real-data experiments, although the true effects in the latter remain unknown (cf. Table 4). All three methods are applied to all 44 experiments. The exponential growth model detects 40 effects with $\Delta_{0.05}^{X_1^2}$ and 31 with $\Delta_{0.05}^{\text{Cant}}$, while the paired t -test also detects 40 effects. The exponential growth model with quantile $\Delta_{0.05}^{X_1^2}$ and the t -test share only one experiment which both methods flag as non-growth-altering. The exponential growth model with adapted threshold $\Delta_{0.05}^{\text{Cant}}$, however, classifies the same seven experiments as non-growth-altering as the other two methods, plus six additional ones (cf. Figure 14, Appendix B). There is no clear pattern in the classification of non-growth-altering effects with respect to sample size, although the exponential growth model with adapted threshold $\Delta_{0.05}^{\text{Cant}}$ is more balanced in flagging experiments with both small and large sample sizes as non-growth-altering. In view of the results of the simulation study, this approach is particularly useful when false positive classifications should be avoided. Nevertheless, the method may fail to detect some existing knockout effects (cf. Figure 5).

We further find for the experiments in PDX models that a separate consideration of the sgRNAs used for a knockout seems reasonable, as the sgRNAs might differ in their knockout efficacy according to the exponential growth model. The confidence interval $\text{CI}_{0.95}^{\text{Cant}}(\theta_1^{(e)})$ can be calculated for these small sample size settings while reflecting parameter uncertainty more appropriately. The logistic growth model, in contrast, requires bootstrapping to compute the confidence interval $\text{CI}_{1-\alpha}^{\text{boot}}(\theta_2^{(l)} - \theta_1^{(l)})$. This approach is not only computationally more intensive but also infeasible for sample sizes that are too small, which applies to several of the separated data sets.

Another drawback of the logistic growth model is, especially for the experiments in PDX models, that parameter values need to be fixed. Although the absolute input value of a knockout experiment can be seen as initial condition $\theta_4^{(l)} = x_1(0)$ for an ODE model, the number of cells homing ultimately in the bone marrow differs between experiments (Ebinger et al, 2016; Bahrami et al, 2023). Moreover, the maximum cell

numbers are rough guesses for the carrying capacity $\theta_3^{(l)} = K$. These determinations further affect the estimation results. Based on our preliminary estimations, we expect the same technical difficulties with an analogue two-dimensional Gompertz growth model (cf. [Laird, 1964](#)) due to its similarity to the logistic growth model. Nevertheless, a logistic or a Gompertz growth model might be useful, if, for example, absolute cell numbers are available. The same might apply to other dynamic growth models that have been used in the past to model cancer growth (e.g. [Benzekry et al, 2014](#)).

A general limitation of our approach is that we disregard that one input and one output measurement belong to one mouse and we neglect individual specific effects of mice in our analysis. To account for that, one might have incorporated mixed effects in the growth models (cf. [Guedj et al, 2007](#); [Lavielle et al, 2011](#); [Wang et al, 2014](#)). However, this would have come along with the challenge to estimate the associated parameters given the number of only two observations per mouse, particularly in light of the fact that estimation of the error parameter $\theta_3^{(e)}$ already fails for the exponential growth model. Moreover, we find that the evaluations of the PDX models of each gene knockout are at least not contradictory in the sense that they share the same effect direction. For this reason, we omitted individual-specific effects.

In conclusion, we showed that a dynamic model provides a more informative approach to analyse time-resolved data than a non-dynamic statistical test. In our application, an exponential growth model turns out to be better suited for evaluating the considered gene modification experiments of leukaemia cells than a logistic growth model. The exponential growth model provides reasonable results even for the smallest sample size settings. Therefore, this growth model can serve as a basis to optimise the experimental design of such experiments so that as few mice as necessary are used and measurement times are allocated effectively.

Acknowledgements. We would like to thank Thanh Thao Bui for her valuable assistance in implementing the models.

Author contributions. Conceptualisation: Julian Wäsche, Christiane Fuchs; Formal analysis: Julian Wäsche; Funding acquisition: Christiane Fuchs, Irmela Jeremias; Investigation: Romina Ludwig, Irmela Jeremias; Methodology: Julian Wäsche, Christiane Fuchs; Supervision: Christiane Fuchs; Visualisation: Julian Wäsche; Writing - original draft preparation: Julian Wäsche; Writing - review and editing: Julian Wäsche, Christiane Fuchs, Romina Ludwig, Irmela Jeremias.

Data availability. All simulations and all statistical analyses were performed in R (Version 4.5.0, [R Core Team, 2025](#)). Code for the statistical analyses, analysis results and the data for the simulation study are available at https://github.com/fuchslab/Modelling_Evaluation_Leukaemia_Trials.

Funding. The project “Opti-Trials” underlying this publication was funded by the German Federal Ministry of Research, Technology and Space (BMFTR) under grant number 16DKWN112A. The responsibility for the content of this publication lies solely with the author(s). Co-funded by the European Union – NextGenerationEU.

Declarations

Conflicts of interest. The authors declare no conflicts of interest.

Compliance with ethical standards. Written consent forms were obtained from all patients and from parents/carers in cases where patients were minors. The study was performed following the ethical standards of the responsible committee on human experimentation (written approval by Ethikkommission des Klinikums der Ludwig-Maximilians-Universität München, ethikkommission@med.uni-muenchen.de, April 15/2008, number 068-08, 222-10) and with the Helsinki Declaration of 1975, as revised in 2013. All animal trials were performed by the current ethical standards of the official committee on animal experimentation written approval by Regierung von Oberbayern, ROB-55.2Vet-2532.Vet.02-15-193, ROB-55.2Vet-2532.Vet.03-16-56, ROB-55.2-2532.Vet.02-20-221 and ROB-55.2Vet-2532.Vet.02-16-7, ROB-55.2-2532.Vet.02-20-159, ROB-55.2-2532.Vet.0321-9, ROB-55.2-2532.Vet.02-23-78).

References

Anstett-Collin F, Denis-Vidal L, Millérioux G (2020) A priori identifiability: an overview on definitions and approaches. *Annual Reviews in Control* 50:139–149. <https://doi.org/10.1016/j.arcontrol.2020.10.006>

Bahrami E, Schmid JP, Jurinovic V, et al (2023) Combined proteomics and CRISPR–Cas9 screens in PDX identify ADAM10 as essential for leukemia *in vivo*. *Molecular Cancer* 22(107). <https://doi.org/10.1186/s12943-023-01803-0>

Banga JR, Villaverde AF (2025) Mechanistic dynamic modelling of biological systems: the road ahead. *Current Opinion in Systems Biology* 42. <https://doi.org/10.1016/j.coisb.2025.100553>

Benzekry S, Lamont C, Beheshti A, et al (2014) Classical mathematical models for description and prediction of experimental tumor growth. *PLoS Computational Biology* 10(8). <https://doi.org/10.1371/journal.pcbi.1003800>

Cao Y, Gillespie DT, Petzold LR (2006) Efficient step size selection for the tau-leaping simulation method. *Journal of Chemical Physics* 124(4). <https://doi.org/10.1063/1.2159468>

Chulián S, Martínez-Rubio, Rosa M, et al (2022) Mathematical models of leukaemia and its treatment: a review. *SeMA Journal* 79:441–486. <https://doi.org/10.1007/s40324-022-00296-z>

Dempster JM, Boyle I, Vazquez F, et al (2021) Chronos: a cell population dynamics model of CRISPR experiments that improves inference of gene fitness effects. *Genome Biology* 22(343). <https://doi.org/10.1186/s13059-021-02540-7>

Ebinger S, Özdemir EZ, Ziegenhain C, et al (2016) Characterization of rare, dormant, and therapy-resistant cells in acute lymphoblastic leukemia. *Cancer Cell* 30(6):849–862. <https://doi.org/10.1016/j.ccr.2016.11.002>

Gao H, Korn JM, Ferretti S, et al (2015) High-throughput screening using patient-derived tumor xenografts to predict clinical trial drug response. *Nature Medicine* 21(11):1318–1325. <https://doi.org/10.1038/nm.3954>

Ghalandary M, Gao Y, Amend D, et al (2023) WT1 and DNMT3A play essential roles in the growth of certain patient AML cells in mice. *Blood* 141(8):955–960. <https://doi.org/10.1182/blood.2022016411>

Gillespie DT (1976) A general method for numerically simulating the stochastic time evolution of coupled chemical reactions. *Journal of Computational Physics* 22:403–434. [https://doi.org/10.1016/0021-9991\(76\)90041-3](https://doi.org/10.1016/0021-9991(76)90041-3)

Gillespie DT (1977) Exact stochastic simulation of coupled chemical reactions. *The Journal of Physical Chemistry* 81(25):2340–2361. <https://doi.org/10.1021/j100540a008>

Guedj J, Thiébaut R, Commenges D (2007) Maximum likelihood estimation in dynamical models of HIV. *Biometrics* 63(4):1198–1206. <https://doi.org/10.1111/j.1541-0420.2007.00812.x>

Hidalgo M, Amant F, Biankin AV, et al (2014) Patient-derived xenograft models: an emerging platform for translational cancer research. *Cancer Discovery* 4(9):998–1013. <https://doi.org/10.1158/2159-8290.CD-14-0001>

Hoffmann H, Thiede C, Glauche I, et al (2020) Differential response to cytotoxic therapy explains treatment dynamics of acute myeloid leukaemia patients: insights from a mathematical modelling approach. *Journal of the Royal Society Interface* 17(170). <https://doi.org/10.1098/rsif.2020.0091>

Kaschek D, Mader W, Kaschek MF, et al (2019) Dynamic modeling, parameter estimation, and uncertainty analysis in R. *Journal of Statistical Software* 88(10). <https://doi.org/10.18637/jss.v088.i10>

Kot M (2001) Elements of Mathematical Ecology. Cambridge University Press, Cambridge

Kreutz C, Bartolome Rodriguez MM, Maiwald T, et al (2007) An error model for protein quantification. *Bioinformatics* 23(20):2747–2753. <https://doi.org/10.1093/bioinformatics/btm397>

Kuang Y, Nagy JD, Eikenberry SE (2016) Introduction to mathematical oncology, 1st edn. Chapman & Hall/CRC, New York

Laird AK (1964) Dynamics of tumor growth. *British Journal of Cancer* 18:490–502.
<https://doi.org/10.1038/bjc.1964.55>

Lavielle M, Samson A, Karina Fermin A, et al (2011) Maximum likelihood estimation of long-term HIV dynamic models and antiviral response. *Biometrics* 67(1):250–259.
<https://doi.org/10.1111/j.1541-0420.2010.01422.x>

Li W, Xu H, Xiao T, et al (2014) MAGeCK enables robust identification of essential genes from genome-scale CRISPR/Cas9 knockout screens. *Genome Biology* 15.
<https://doi.org/10.1186/s13059-014-0554-4>

Li W, Köster J, Xu H, et al (2015) Quality control, modeling, and visualization of CRISPR screens with MAGeCK-VISPR. *Genome Biology* 16. <https://doi.org/10.1186/s13059-015-0843-6>

Meyers RM, Bryan JG, McFarland JM, et al (2017) Computational correction of copy number effect improves specificity of CRISPR-Cas9 essentiality screens in cancer cells. *Nature Genetics* 49(12):1779–1784. <https://doi.org/10.1038/ng.3984>

Pineda-Krch M (2008) GillespieSSA: implementing the stochastic simulation algorithm in R. *Journal of Statistical Software* 25(12). <https://doi.org/10.18637/jss.v025.i12>

R Core Team (2025) R: a language and environment for statistical computing. URL <https://www.R-project.org/>

Raue A, Kreutz C, Maiwald T, et al (2009) Structural and practical identifiability analysis of partially observed dynamical models by exploiting the profile likelihood. *Bioinformatics* 25(15):1923–1929. <https://doi.org/10.1093/bioinformatics/btp358>

Raue A, Becker V, Klingmüller U, et al (2010) Identifiability and observability analysis for experimental design in nonlinear dynamical models. *Chaos* 20(4). <https://doi.org/10.1063/1.3528102>

Riesle AJ, Gao M, Rosenblatt M, et al (2023) Activator-blocker model of transcriptional regulation by pioneer-like factors. *Nature Communications* 14. <https://doi.org/10.1038/s41467-023-41507-z>

Shalem O, Sanjana NE, Hartenian E, et al (2014) Genome-scale CRISPR-Cas9 knockout screening in human cells. *Science* 343(6166):84–87. <https://doi.org/10.1126>

science.1247005

Siegel RL, Miller KD, Wagle NS, et al (2023) Cancer statistics, 2023. CA: A Cancer Journal for Clinicians 73(1):17–48. <https://doi.org/10.3322/caac.21763>

Tönsing C, Steiert B, Timmer J, et al (2023) Likelihood-ratio test statistic for the finite-sample case in nonlinear ordinary differential equation models. PLoS Computational Biology 19(9). <https://doi.org/10.1371/journal.pcbi.1011417>

Wang L, Cao J, Ramsay JO, et al (2014) Estimating mixed-effects differential equation models. Statistics and Computing 24:111–121. <https://doi.org/10.1007/s11222-012-9357-1>

Wieland FG, Hauber AL, Rosenblatt M, et al (2021) On structural and practical identifiability. Current Opinion in Systems Biology 25:60–69. <https://doi.org/10.1016/j.coisb.2021.03.005>

Wilkinson DJ (2019) Stochastic Modelling for Systems Biology, 3rd edn. Chapman & Hall/CRC, Boca Raton

Appendix A Complementary tables

Table 3: Overview of all gene modification experiments that are analysed. From left to right: leukaemia sample name, identifier of knocked-out gene, number of sgRNAs used, sample size, maximum number of cells in the sample that have ever been measured in the bone marrow (BM) of a PDX model in the laboratory where the experiments were conducted (in million), absolute number of input cells (in thousands), and *p*-value for the two *t*-tests comparing input measurements from day zero with corresponding measurements from (approx.) day 14 and a variable end day

Sample	Gene	#sgRNAs	Details of experiment			<i>p</i> -value of <i>t</i> -tests	
			Sample size	Max. cell number	Input value	day 14	end day
ALL-1034	1	3	18	110	33	0.001	0.006
ALL-1034	2	3	18	110	33	0.008	0.001
ALL-1034	3	3	18	110	33	0.000	0.000
ALL-1034	4	3	18	110	33	0.006	0.004
ALL-1034	5	3	20	110	33	0.000	0.000
ALL-1034	6	1	4	110	33	-	0.747
ALL-1034	7	3	20	110	33	0.000	0.000
ALL-199	1	3	20	70	400	0.000	0.000
ALL-199	2	3	20	70	400	0.000	0.023
ALL-199	3	3	20	70	400	0.033	0.000
ALL-199	4	3	20	70	400	0.017	0.012
ALL-199	5	3	20	70	400	0.000	0.000
ALL-199	7	3	20	70	400	0.000	0.000
ALL-265	1	3	20	70	100	0.000	0.000
ALL-265	2	3	16	70	100	0.001	0.000
ALL-265	3	3	16	70	100	0.000	0.000
ALL-265	5	2	8	70	100	0.004	0.013
ALL-265	7	3	12	70	100	0.007	0.023
ALL-50	1	3	14	260	30	0.000	0.000
ALL-50	2	3	14	260	30	0.015	0.000
ALL-50	3	3	14	260	30	0.000	0.000
ALL-50	4	3	12	260	30	0.053	0.025
ALL-50	5	3	18	260	30	0.001	0.000
ALL-50	6	1	6	260	30	-	0.168
ALL-50	7	3	18	260	30	0.003	0.000
ALL-502	1	3	16	100	40	0.219	0.004
ALL-502	2	3	12	100	40	0.073	0.026
ALL-502	3	3	20	100	40	0.012	0.002
ALL-502	4	3	16	100	40	0.013	0.009
ALL-502	5	3	18	100	40	0.003	0.016
ALL-502	6	1	4	100	40	-	0.407
ALL-502	7	3	20	100	40	0.000	0.000
AML-356	1	3	22	70	400	0.001	0.000
AML-356	2	3	6	70	400	-	0.018
AML-356	3	3	6	70	400	-	0.013
AML-356	5	3	20	70	400	0.000	0.000
AML-356	7	3	20	70	400	0.000	0.000
AML-388	1	3	16	80	400	0.099	0.018
AML-388	2	3	20	80	400	0.013	0.006
AML-388	3	3	20	80	400	0.000	0.000
AML-388	4	3	16	80	400	0.105	0.161
AML-388	5	3	20	80	400	0.010	0.015
AML-388	6	1	4	80	400	-	0.009
AML-388	7	3	20	80	400	0.000	0.001

Table 4: Overview of estimation results of the exponential growth model for knockout experiments in PDX models including parameter estimates for $\hat{\theta}^{(e)}$ and profile likelihood-based 95 % confidence intervals $CI_{0.95}^{\text{Cant}}(\theta_j^{(e)})$ with adapted threshold $\Delta_{0.05}^{\text{Cant}} = 7.16$. For experiments for which significant growth-altering effects are recognised, i.e. for which $CI_{0.95}^{\text{Cant}}(\theta_1^{(e)}) \subset \mathbb{R}_+$ or $CI_{0.95}^{\text{Cant}}(\theta_1^{(e)}) \subset \mathbb{R}_-$, the confidence interval is marked with a star

Experiment		Parameter estimates			Confidence intervals		
Sample	Gene	$\hat{\theta}_1^{(e)}$	$\hat{\theta}_2^{(e)}$	$\hat{\theta}_3^{(e)}$	$CI_{0.95}^{\text{Cant}}(\theta_1^{(e)})$	$CI_{0.95}^{\text{Cant}}(\theta_2^{(e)})$	$CI_{0.95}^{\text{Cant}}(\theta_3^{(e)})$
ALL-1034	1	0.027	1.108	0.454	[0.004, 0.054]*	[0.377, 2.009]	[0.308, 0.766]
ALL-1034	2	0.047	1.199	0.539	[0.026, 0.074]*	[0.341, 2.303]	[0.366, 0.908]
ALL-1034	3	0.081	0.922	0.950	[0.045, 0.143]*	[0.012, 2.701]	[0.648, 1.548]
ALL-1034	4	0.049	1.088	0.942	[0.006, 0.134]*	(0, 3.212]	[0.64, 1.561]
ALL-1034	5	0.090	0.801	1.016	[0.051, 0.176]*	[0.001, 2.534]	[0.706, 1.599]
ALL-1034	6	0.001	1.022	0.024	[-0.004, 0.005]	[0.876, 1.173]	[0.011, 0.091]
ALL-1034	7	0.072	0.734	1.263	[0.023, ∞)*	(0, 2.996]	[0.883, 1.943]
ALL-199	1	0.086	1.441	0.872	[0.063, 0.113]*	[0.266, 3.272]	[0.605, 1.395]
ALL-199	2	0.025	0.713	0.525	[0.007, 0.05]*	[0.103, 1.474]	[0.362, 0.858]
ALL-199	3	0.112	0.050	1.185	[0.067, ∞)*	(0, 0.789]	[0.851, 1.742]
ALL-199	4	0.027	0.872	0.510	[0.009, 0.05]*	[0.207, 1.689]	[0.352, 0.833]
ALL-199	5	0.081	0.560	2.372	[0.028, ∞)*	(0, 4.815]	[1.786, 3.188]
ALL-199	7	0.108	0.536	1.450	[0.072, ∞)*	(0, 2.457]	[1.031, 2.145]
ALL-265	1	0.083	1.409	1.182	[0.054, 0.117]*	[0.092, 4.141]	[0.824, 1.826]
ALL-265	2	0.057	1.218	0.525	[0.041, 0.076]*	[0.36, 2.318]	[0.349, 0.917]
ALL-265	3	0.103	1.510	0.732	[0.082, 0.126]*	[0.351, 3.246]	[0.488, 1.258]
ALL-265	5	0.072	1.041	1.503	$(-\infty, -0.286] \cup [-0.007, \infty)$	(0, 8.676]	[0.888, 2.809]
ALL-265	7	0.039	1.055	1.194	$(-\infty, -0.485] \cup [-0.018, \infty)$	(0, 4.858]	[0.756, 2.146]
ALL-50	1	0.080	1.402	1.358	[0.041, 0.259]*	(0, 5.97]	[0.894, 2.259]
ALL-50	2	0.042	1.678	0.343	[0.031, 0.054]*	[0.854, 2.636]	[0.223, 0.629]
ALL-50	3	0.084	0.990	1.152	[0.05, ∞)*	(0, 3.806]	[0.756, 1.972]
ALL-50	4	0.031	0.471	2.067	$(-\infty, \infty)$	(0, 8.482]	[1.345, 3.041]
ALL-50	5	0.070	0.602	1.856	[0.027, ∞)*	(0, 4.835]	[1.306, 2.696]
ALL-50	6	0.004	1.016	0.076	[-0.002, 0.011]	[0.702, 1.356]	[0.041, 0.212]
ALL-50	7	0.041	1.265	0.521	[0.027, 0.058]*	[0.38, 2.38]	[0.353, 0.877]
ALL-502	1	0.050	1.014	0.410	[0.031, 0.074]*	[0.346, 1.821]	[0.272, 0.718]
ALL-502	2	0.018	1.329	0.753	[-0.034, 0.082]	(0, 3.728]	[0.474, 1.458]
ALL-502	3	0.018	1.196	0.624	[-0.009, 0.046]	[0.238, 2.441]	[0.43, 1.019]
ALL-502	4	0.023	1.465	0.650	[-0.008, 0.059]	[0.226, 3.174]	[0.432, 1.136]
ALL-502	5	0.015	2.126	0.301	[-0.001, 0.031]	[1.345, 3.006]	[0.204, 0.507]
ALL-502	6	0.003	1.004	0.031	[-0.002, 0.008]	[0.814, 1.203]	[0.015, 0.12]
ALL-502	7	0.077	1.030	0.605	[0.049, 0.111]*	[0.257, 2.091]	[0.418, 0.985]
AML-356	1	0.101	0.573	0.655	[0.064, 0.158]*	[0.07, 1.372]	[0.46, 1.034]
AML-356	2	0.160	0.597	0.936	[0.089, ∞)*	(0, 6.108]	[0.507, 2.245]
AML-356	3	0.186	1.303	0.122	[0.176, 0.199]*	[0.744, 1.942]	[0.065, 0.341]
AML-356	5	0.118	0.724	1.678	[0.05, 0.373]*	(0, 3.771]	[1.202, 2.424]
AML-356	7	0.078	0.445	1.839	$(-\infty, -0.232] \cup [-0.008, \infty)$	(0, 3.37]	[1.327, 2.608]
AML-388	1	0.042	0.706	0.271	[0.011, 0.082]*	[0.273, 1.209]	[0.18, 0.475]
AML-388	2	0.032	1.003	0.335	[0, 0.067]	[0.475, 1.628]	[0.231, 0.547]
AML-388	3	0.093	1.004	0.464	[0.056, 0.139]*	[0.355, 1.853]	[0.32, 0.756]
AML-388	4	0.063	1.018	0.712	[-0.002, 0.188]	[0.011, 2.785]	[0.473, 1.245]
AML-388	5	0.052	0.924	0.468	[0.01, 0.105]*	[0.266, 1.778]	[0.323, 0.765]
AML-388	6	-0.007	1.114	0.005	[-0.009, -0.005]*	[1.084, 1.145]	[0.002, 0.018]
AML-388	7	0.068	1.044	0.522	[0.025, 0.124]*	[0.278, 2.07]	[0.361, 0.853]

Table 5: Overview of estimation results of the logistic growth model for knockout experiments in PDX models including parameter estimates for $\hat{\theta}^{(l)}$ and profile likelihood-based 95 % confidence intervals $CI_{0.95}^{\chi^2_1}(\theta_j^{(l)})$, where the values of $\hat{\theta}_5^{(l)} = \hat{x}_2(0)$ and $CI_{0.95}^{\chi^2_1}(\theta_5^{(l)})$ are shown in thousands. The parameter $\theta_4^{(l)} = x_1(0)$ is set to the input value of the specific PDX sample engrafted into mice and $\theta_3^{(l)} = K$ is set to the maximum number of cells that has ever been measured for the specific PDX sample in the laboratory performing the knockout experiments. For experiments for which significant growth-altering effects are recognised, i.e. for which $CI_{0.95}^{\text{boot}}(\lambda_2 - \lambda_1) \subset \mathbb{R}_+$ or $CI_{0.95}^{\text{boot}}(\lambda_2 - \lambda_1) \subset \mathbb{R}_-$, the confidence interval is marked with a star

Experiment		Parameter estimates				Confidence intervals				
Sample	Gene	$\hat{\lambda}_1$	$\hat{\lambda}_2$	$\hat{x}_2(0)$	$\hat{\sigma}$	$CI_{0.95}^{\chi^2_1}(\lambda_1)$	$CI_{0.95}^{\chi^2_1}(\lambda_2)$	$CI_{0.95}^{\chi^2_1}(x_2(0))$	$CI_{0.95}^{\chi^2_1}(\sigma)$	$CI_{0.95}^{\text{boot}}(\lambda_2 - \lambda_1)$
ALL-1034	1	0.708	0.881	25.651	0.301	[0.374, ∞)	[1.6, ∞)	[14.071, 38.47]	[0.223, 0.432]	[0.11, 0.246]*
ALL-1034	2	0.279	0.415	27.063	0.431	[0.175, 0.439]	[1.292, 1.866]	[10.27, 46.481]	[0.321, 0.622]	[0.051, 0.179]*
ALL-1034	3	0.218	0.481	11.553	0.730	[0.141, 0.342]	[1.358, ∞)	(0, 37.685]	[0.546, 1.054]	[0.174, 0.316]*
ALL-1034	4	0.493	0.725	20.618	0.769	[0.234, ∞)	[1.406, ∞)	(0, 54.652]	[0.574, 1.111]	[0.095, 0.342]*
ALL-1034	5	0.228	0.493	9.829	0.871	[0.137, 0.387]	[1.329, ∞)	(0, 38.947]	[0.661, 1.225]	[0.159, 0.326]*
ALL-1034	7	0.469	0.904	7.409	0.921	[0.252, ∞)	[1.615, ∞)	(0, 36.223]	[0.701, 1.285]	[0.261, 0.618]*
ALL-199	1	-0.029	0.221	264.446	0.521	[−0.045, −0.009]	[1.18, 1.378]	[52.859, 513.886]	[0.394, 0.736]	[0.201, 0.303]*
ALL-199	2	0.158	0.249	200.768	0.491	(− ∞ , ∞)	[0, ∞)	[19.317, 411.007]	[0.371, 0.694]	[0.022, 0.107]*
ALL-199	3	-0.065	0.047	21.611	1.182	[−0.517, 0.063]	[0.664, ∞)	(0, 195.03]	[0.928, 1.575]	[0.023, 0.163]*
ALL-199	4	0.134	0.209	273.092	0.487	[−0.548, 0.384]	[0.59, 1.61]	[72.272, 507.086]	[0.368, 0.688]	[0.001, 0.109]*
ALL-199	5	-0.152	0.832	30.036	1.227	[−2.956, −0.036]	[1.489, ∞)	(0, 353.835]	[0.963, 1.641]	[0.639, 1.419]*
ALL-199	7	-0.053	0.298	24.075	1.267	[−0.112, −0.005]	[1.15, ∞)	(0, 316.81]	[1.002, 1.69]	[0.238, 0.472]*
ALL-265	1	0.013	0.280	56.522	0.743	[−0.011, 0.05]	[1.225, ∞)	(0, 145.747]	[0.562, 1.051]	[0.234, 0.308]*
ALL-265	2	0.063	0.176	85.480	0.469	[−0.49, −0.421] \cup [0.013, 0.102]	[0.652, 0.666] \cup [1.073, 1.324]	[25.825, 156.352]	[0.344, 0.694]	[0.093, 0.133]*
ALL-265	3	-0.029	0.193	74.399	0.462	[−0.042, −0.016]	[1.156, 1.313]	[19.083, 139.78]	[0.339, 0.683]	[0.193, 0.249]*
ALL-265	5	0.106	0.464	36.575	0.983	[0.019, 3.802]	[1.255, ∞)	(0, 241.612]	[0.654, 1.678]	[0.121, 0.475]*
ALL-265	7	0.396	0.788	48.645	0.731	[0.17, ∞)	[1.431, ∞)	(0, 162.93]	[0.515, 1.155]	[0.159, 0.634]*
ALL-50	1	0.152	0.503	22.903	0.508	[0.111, 0.212]	[1.505, 1.908]	[3.277, 46.896]	[0.365, 0.775]	[0.272, 0.405]*
ALL-50	2	0.192	0.298	38.533	0.230	[0.138, 0.247]	[1.237, 1.466]	[26.597, 51.632]	[0.165, 0.35]	[0.094, 0.119]*
ALL-50	3	0.139	0.452	8.861	0.851	[0.081, 0.257]	[1.307, ∞)	(0, 40.879]	[0.617, 1.283]	[0.265, 0.365]*
ALL-50	4	0.541	1.002	5.279	1.505	[0.27, 9.901]	[1.607, ∞)	(0, 69.372]	[1.102, 2.143]	[0.127, 0.755]*
ALL-50	5	0.334	0.905	4.926	1.284	[0.186, 7.033]	[1.698, ∞)	(0, 43.885]	[0.98, 1.759]	[0.132, 0.915]*
ALL-50	7	0.285	0.437	26.281	0.377	[0.191, 0.389]	[1.334, 1.809]	[12.443, 41.993]	[0.281, 0.543]	[0.126, 0.181]*
ALL-502	1	-0.028	0.022	40.598	0.410	[−0.614, 0.2]	[0.563, 1.352]	[19.171, 62.406]	[0.3, 0.606]	[0.003, 0.06]*
ALL-502	2	0.626	0.811	32.458	0.560	[0.272, ∞)	[1.424, ∞)	[0.774, 73.037]	[0.393, 0.883]	[0.042, 0.32]*
ALL-502	3	0.644	0.800	31.672	0.496	[0.292, ∞)	[1.44, ∞)	[9.948, 57.114]	[0.374, 0.699]	[0.043, 0.261]*
ALL-502	4	0.650	0.833	39.378	0.480	[0.297, ∞)	[1.471, ∞)	[13.371, 70.429]	[0.351, 0.707]	[0.055, 0.284]*
ALL-502	5	0.524	0.581	75.329	0.262	[−0.753, −0.711] \cup [0.188, ∞)	[0.483, 0.497] \cup [1.232, ∞)	[55.419, 97.181]	[0.195, 0.377]	[0.004, 0.091]*
ALL-502	7	0.179	0.320	28.086	0.553	[−0.712, −0.648] \cup [0.077, 0.269]	[0.529, 0.547] \cup [1.163, 1.625]	[5.157, 55.413]	[0.417, 0.781]	[0.116, 0.17]*
AML-356	1	0.076	0.236	147.303	0.642	[−1.419, 0.148]	[0.437, ∞)	(0, 391.884]	[0.492, 0.893]	[0.106, 0.209]*
AML-356	5	0.044	0.593	39.409	1.229	[−0.029, 1.724]	[1.384, ∞)	(0, 415.516]	[0.959, 1.653]	[0.117, 0.699]*
AML-356	7	0.213	0.944	26.754	1.327	[0.08, 3.409]	[1.528, ∞)	(0, 347.144]	[1.051, 1.756]	[0.359, 1.239]*
AML-388	1	-0.083	-0.040	282.441	0.271	[−1.501, 0.236]	[0.312, 1.35]	[163.405, 418.893]	[0.199, 0.401]	[0.021, 0.063]*
AML-388	2	0.561	0.692	344.553	0.286	[−1.375, −1.246] \cup [0.211, ∞)	[0.264, 0.297] \cup [1.303, ∞)	[211.881, 490.064]	[0.216, 0.401]	[0.035, 0.212]*
AML-388	3	0.250	0.454	305.593	0.346	[0.149, ∞)	[1.336, ∞)	[154.351, 474.206]	[0.261, 0.488]	[0.018, 0.26]*
AML-388	4	0.115	0.189	392.960	0.711	[−2.694, ∞)	[0, ∞)	[18.752, 868.262]	[0.522, 1.053]	[−0.019, 0.114]
AML-388	5	0.483	0.665	303.076	0.412	[−1.414, −1.202] \cup [0.159, ∞)	[0.261, 0.311] \cup [1.255, ∞)	[124.638, 506.313]	[0.311, 0.581]	[0.057, 0.301]*
AML-388	7	0.334	0.502	345.361	0.471	(− ∞ , −1.189] \cup [0.092, ∞)	[0, 0.344] \cup [1.169, ∞)	[130.342, 595.464]	[0.356, 0.666]	[0.03, 0.258]*

Table 6: Overview of estimation results of the exponential growth model for knockout experiments in PDX models, with one growth model estimated for each of the up to three sgRNAs s used. Included are parameter estimates for $\hat{\theta}^{(e)}$ and profile likelihood-based 95 % confidence intervals $CI_{0.95}^{Cant}(\theta_j^{(e)})$ with adapted threshold $\Delta_{0.05}^{Cant} = 7.16$. For experiments for which significant growth-altering effects are recognised, i.e. for which $CI_{0.95}^{Cant}(\theta_1^{(e)}) \subset \mathbb{R}_+$ or $CI_{0.95}^{Cant}(\theta_1^{(e)}) \subset \mathbb{R}_-$, the confidence interval is marked with a star

Experiment			Parameter estimates			Confidence intervals			<i>p</i> -value of <i>t</i> -tests		
Sample	Gene	s	$\hat{\theta}_1^{(e)}$	$\hat{\theta}_2^{(e)}$	$\hat{\theta}_3^{(e)}$	$CI_{0.95}^{Cant}(\theta_1^{(e)})$	$CI_{0.95}^{Cant}(\theta_2^{(e)})$	$CI_{0.95}^{Cant}(\theta_3^{(e)})$	day	14	end day
ALL-1034	1	1	0.011	1.207	0.542	$(-\infty, \infty)$	$(0, 5.598]$	$[0.263, 1.905]$	-	-	
ALL-1034	1	2	0.028	1.059	0.551	$(-\infty, -0.652] \cup [-0.05, \infty)$	$(0, 3.807]$	$[0.298, 1.518]$	-	0.280	
ALL-1034	1	3	0.035	1.120	0.228	$[0.014, 0.057]^*$	$[0.488, 1.869]$	$[0.131, 0.535]$	0.018	0.039	
ALL-1034	2	1	0.062	1.394	0.215	$[0.035, 0.096]^*$	$[0.294, 2.88]$	$[0.104, 0.833]$	-	-	
ALL-1034	2	2	0.045	0.891	0.546	$[-0.005, \infty)$	$(0, 3.371]$	$[0.295, 1.499]$	-	0.184	
ALL-1034	2	3	0.045	1.418	0.534	$[0.007, 0.095]^*$	$[0.058, 3.573]$	$[0.309, 1.248]$	0.026	0.019	
ALL-1034	3	1	0.073	1.301	0.539	$[0.008, 0.471]^*$	$[0, 5.343]$	$[0.262, 1.936]$	-	-	
ALL-1034	3	2	0.110	1.106	0.351	$[0.083, 0.15]^*$	$[0.147, 2.595]$	$[0.19, 0.977]$	-	0.001	
ALL-1034	3	3	0.053	1.096	1.047	$(-\infty, -0.368] \cup [-0.031, \infty)$	$(0, 5.546]$	$[0.609, 2.207]$	0.023	0.057	
ALL-1034	4	1	0.008	0.836	1.321	$(-\infty, \infty)$	$(0, 16.113]$	$[0.643, 2.979]$	-	-	
ALL-1034	4	2	0.079	1.491	0.488	$[0.038, 0.152]^*$	$[0.011, 4.264]$	$[0.264, 1.352]$	-	0.005	
ALL-1034	4	3	0.033	1.613	0.466	$[-0.006, 0.079]$	$[0.18, 3.694]$	$[0.269, 1.094]$	0.119	0.094	
ALL-1034	5	1	0.124	1.208	0.278	$[0.099, 0.155]^*$	$[0.324, 2.436]$	$[0.15, 0.777]$	-	0.001	
ALL-1034	5	2	0.039	1.349	0.534	$[-0.014, 0.363]$	$(0, 4.324]$	$[0.288, 1.478]$	-	0.040	
ALL-1034	5	3	0.098	1.305	0.785	$[0.043, 0.188]^*$	$[0, 4.465]$	$[0.456, 1.745]$	0.023	0.011	
ALL-1034	7	1	0.070	0.966	1.221	$(-\infty, \infty)$	$(0, 8.605]$	$[0.669, 2.703]$	-	0.019	
ALL-1034	7	2	0.037	1.149	0.453	$[-0.009, 0.153]$	$(0, 3.361]$	$[0.244, 1.26]$	-	0.019	
ALL-1034	7	3	0.102	1.190	1.103	$[0.025, 0.613]^*$	$[0, 6.066]$	$[0.645, 2.293]$	0.003	0.013	
ALL-199	1	1	0.071	1.275	0.331	$[0.04, 0.119]^*$	$[0.01, 3.436]$	$[0.16, 1.268]$	-	-	
ALL-199	1	2	0.089	1.661	0.763	$[0.053, 0.14]^*$	$[0.022, 5.087]$	$[0.443, 1.71]$	0.024	0.008	
ALL-199	1	3	0.090	1.698	0.920	$[0.046, 0.162]^*$	$[0, 6.223]$	$[0.535, 2.007]$	0.012	0.012	
ALL-199	2	1	0.043	0.837	0.140	$[0.036, 0.052]^*$	$[0.511, 1.196]$	$[0.081, 0.328]$	0.031	0.000	
ALL-199	2	2	0.006	0.857	0.217	$[-0.014, 0.023]$	$[0.315, 1.481]$	$[0.125, 0.51]$	0.050	0.219	
ALL-199	2	3	0.012	1.173	0.284	$[-0.036, 0.059]$	$(0, 3.061]$	$[0.138, 1.102]$	-	-	
ALL-199	3	1	0.134	0.060	1.026	$[0.074, \infty)^*$	$[0, 1.308]$	$[0.621, 1.974]$	0.305	0.012	
ALL-199	3	2	0.050	0.596	0.137	$[0.042, 0.06]^*$	$[0.321, 0.902]$	$[0.079, 0.323]$	0.045	0.023	
ALL-199	3	3	0.110	0.784	0.128	$[0.098, 0.125]^*$	$[0.324, 1.35]$	$[0.062, 0.495]$	-	-	
ALL-199	4	1	0.007	0.861	0.045	$[-0.001, 0.014]$	$[0.639, 1.094]$	$[0.022, 0.174]$	-	-	
ALL-199	4	2	0.034	0.933	0.595	$[-0.002, \infty)$	$(0, 2.88]$	$[0.344, 1.385]$	0.060	0.231	
ALL-199	4	3	0.027	1.040	0.257	$[0.011, 0.045]^*$	$[0.362, 1.847]$	$[0.148, 0.604]$	0.144	0.153	
ALL-199	5	1	0.064	0.541	2.377	$(-\infty, \infty)$	$(0, 13.39]$	$[1.51, 3.68]$	0.006	0.005	
ALL-199	5	2	0.092	0.575	2.205	$(-\infty, \infty)$	$(0, 10.542]$	$[1.4, 3.524]$	0.021	0.012	
ALL-199	5	3	0.098	0.779	2.490	$(-\infty, 0.482]$	$(0, 49.094]$	$[1.372, 4.464]$	-	-	
ALL-199	7	1	0.132	1.571	0.737	$[0.097, 0.173]^*$	$[0.102, 4.617]$	$[0.429, 1.639]$	0.015	0.000	
ALL-199	7	2	0.071	0.594	1.147	$[0.015, \infty)^*$	$[0, 4.058]$	$[0.674, 2.284]$	0.015	0.050	
ALL-199	7	3	0.131	1.641	0.913	$[0.057, 0.357]^*$	$[0, 10.61]$	$[0.448, 2.749]$	-	-	
ALL-265	1	1	0.083	1.468	0.932	$[0.042, 0.168]^*$	$[0, 5.661]$	$[0.542, 2.025]$	0.018	0.011	
ALL-265	1	2	0.057	1.535	1.197	$(-\infty, 0.525]$	$(0, 16.216]$	$[0.587, 3.14]$	-	-	
ALL-265	1	3	0.094	1.785	1.138	$[0.046, 0.185]^*$	$[0, 8.241]$	$[0.664, 2.36]$	0.039	0.007	
ALL-265	2	1	0.053	1.351	0.143	$[0.04, 0.068]^*$	$[0.585, 2.265]$	$[0.069, 0.554]$	-	-	
ALL-265	2	2	0.068	1.337	0.372	$[0.05, 0.089]^*$	$[0.356, 2.631]$	$[0.215, 0.871]$	0.064	0.001	
ALL-265	2	3	0.037	1.558	0.326	$[0.008, 0.079]^*$	$[0, 4.072]$	$[0.158, 1.258]$	-	-	
ALL-265	3	1	0.114	1.757	0.450	$[0.078, 0.165]^*$	$[0.019, 5.459]$	$[0.219, 1.672]$	-	-	
ALL-265	3	2	0.106	1.706	0.695	$[0.076, 0.143]^*$	$[0.115, 4.737]$	$[0.403, 1.568]$	0.031	0.019	
ALL-265	3	3	0.084	1.584	0.488	$[0.045, 0.158]^*$	$[0, 5.44]$	$[0.237, 1.798]$	-	-	
ALL-265	5	1	0.099	1.817	1.309	$(-\infty, 0.507]$	$(0, 20.914]$	$[0.645, 3.333]$	-	-	
ALL-265	5	2	0.044	1.687	1.024	$(-\infty, 0.609]$	$(0, 14.01]$	$[0.499, 2.897]$	-	-	
ALL-265	7	1	0.045	1.360	1.271	$(-\infty, \infty)$	$(0, 17.187]$	$[0.622, 3.168]$	-	-	
ALL-265	7	2	0.016	1.410	0.490	$(-\infty, 0.399]$	$(0, 5.423]$	$[0.238, 1.81]$	-	-	
ALL-265	7	3	0.051	1.467	1.115	$(-\infty, 0.643]$	$(0, 14.217]$	$[0.545, 3.006]$	-	-	
ALL-50	1	1	0.080	1.438	1.136	$[0.022, \infty)^*$	$[0, 9.623]$	$[0.62, 2.628]$	-	0.003	
ALL-50	1	2	0.094	1.479	1.580	$(-\infty, 0.509]$	$(0, 25.474]$	$[0.789, 3.61]$	-	-	
ALL-50	1	3	0.070	1.758	1.129	$(-\infty, 0.514]$	$(0, 15.92]$	$[0.552, 3.072]$	-	-	

ALL-50	2	1	0.033	2.046	0.203	[0.015, 0.053]*	[0.626, 3.828]	[0.098, 0.787]	-	-
ALL-50	2	2	0.048	1.676	0.279	[0.032, 0.066]*	[0.488, 3.21]	[0.151, 0.782]	-	0.003
ALL-50	2	3	0.038	1.560	0.330	[0.008, 0.083]*	[0, 4.09]	[0.16, 1.276]	-	-
ALL-50	3	1	0.065	1.554	0.948	($-\infty$, -0.217] \cup [-0.034, ∞)	(0, 11.073]	[0.463, 2.776]	-	-
ALL-50	3	2	0.101	0.701	1.183	[0.041, ∞)*	[0, 6.305]	[0.652, 2.606]	-	0.004
ALL-50	3	3	0.070	1.608	0.935	($-\infty$, -0.423] \cup [-0.013, ∞)	(0, 11.102]	[0.457, 2.764]	-	-
ALL-50	4	1	0.043	3.788	0.481	[0.003, 0.095]*	[0, 11.501]	[0.233, 1.844]	-	-
ALL-50	4	2	0.025	3.018	0.976	($-\infty$, 0.392]	(0, 20.99]	[0.472, 2.906]	-	-
ALL-50	4	3	0.001	0.192	2.766	($-\infty$, 0.422]	(0, 52.376]	[1.624, 4.3]	-	-
ALL-50	5	1	0.073	0.556	2.424	($-\infty$, ∞)	(0, 25.05]	[1.442, 3.99]	-	0.009
ALL-50	5	2	0.064	1.397	0.891	[0.018, ∞)*	[0, 7.102]	[0.483, 2.239]	-	0.025
ALL-50	5	3	0.064	1.741	1.151	[0.005, ∞)*	[0, 11.601]	[0.625, 2.677]	-	0.015
ALL-50	7	1	0.041	1.238	0.537	[0.01, 0.423]*	[0, 3.967]	[0.29, 1.484]	-	-
ALL-50	7	2	0.048	1.489	0.435	[0.024, 0.088]*	[0.017, 3.824]	[0.235, 1.213]	-	0.018
ALL-50	7	3	0.033	1.319	0.320	[0.014, 0.059]*	[0.166, 2.877]	[0.173, 0.898]	-	0.039
ALL-502	1	1	0.027	2.412	0.290	($-\infty$, 0.011, 0.069]	[0.275, 5.533]	[0.14, 1.125]	-	-
ALL-502	1	2	0.066	0.815	0.237	[0.048, 0.09]*	[0.272, 1.469]	[0.137, 0.558]	0.725	0.013
ALL-502	1	3	0.044	0.776	0.088	[0.031, 0.06]*	[0.391, 1.209]	[0.042, 0.341]	-	-
ALL-502	2	1	0.022	1.330	0.091	[0.01, 0.035]*	[0.793, 1.931]	[0.044, 0.352]	-	-
ALL-502	2	2	0.007	1.250	1.169	($-\infty$, ∞)	(0, 15.79]	[0.566, 2.88]	-	-
ALL-502	2	3	0.025	1.493	0.405	($-\infty$, -0.908] \cup [-0.042, 0.156]	(0, 4.791]	[0.196, 1.55]	-	-
ALL-502	3	1	0.007	1.337	0.202	($-\infty$, 0.033, 0.039]	[0.222, 2.788]	[0.098, 0.786]	-	-
ALL-502	3	2	0.018	1.076	0.871	($-\infty$, ∞)	(0, 4.725]	[0.504, 1.923]	0.304	0.019
ALL-502	3	3	0.022	1.329	0.351	($-\infty$, 0.003, 0.05]	[0.302, 2.651]	[0.203, 0.826]	0.198	0.050
ALL-502	4	1	0.018	1.710	0.167	($-\infty$, 0.006, 0.043]	[0.61, 3.06]	[0.081, 0.648]	-	-
ALL-502	4	2	0.031	1.500	0.792	($-\infty$, -0.718] \cup [-0.042, ∞)	(0, 5.299]	[0.458, 1.812]	0.159	0.042
ALL-502	4	3	0.012	1.499	0.366	($-\infty$, -0.439] \cup [-0.132, 0.104]	(0, 4.528]	[0.178, 1.416]	-	-
ALL-502	5	1	0.011	2.911	0.234	($-\infty$, 0.019, 0.04]	[1.351, 4.815]	[0.126, 0.656]	0.242	-
ALL-502	5	2	0.014	1.582	0.149	($-\infty$, 0.001, 0.028]	[1.029, 2.197]	[0.086, 0.35]	0.127	0.181
ALL-502	5	3	0.026	2.646	0.090	[0.012, 0.039]*	[1.776, 3.62]	[0.043, 0.349]	-	-
ALL-502	7	1	0.061	1.501	0.406	[0.015, 0.117]*	[0.168, 3.565]	[0.219, 1.131]	0.021	-
ALL-502	7	2	0.105	1.138	0.263	[0.083, 0.13]*	[0.473, 1.976]	[0.152, 0.616]	0.057	0.004
ALL-502	7	3	0.055	1.046	0.384	[0.016, 0.136]*	[0, 2.81]	[0.207, 1.072]	-	0.085
AML-356	1	1	0.113	0.798	0.178	[0.094, 0.134]*	[0.418, 1.252]	[0.103, 0.419]	0.017	0.003
AML-356	1	2	0.132	1.101	0.185	[0.107, 0.161]*	[0.533, 1.801]	[0.1, 0.518]	0.034	-
AML-356	1	3	0.067	0.545	0.178	[0.044, 0.096]*	[0.202, 0.959]	[0.103, 0.418]	0.062	0.069
AML-356	5	1	0.209	1.573	1.396	[0.026, 0.52]*	[0, 21.809]	[0.697, 3.456]	-	-
AML-356	5	2	0.116	1.223	1.519	($-\infty$, -0.356] \cup [-0.002, ∞)	(0, 9.726]	[0.903, 2.862]	0.003	0.004
AML-356	5	3	0.073	1.625	0.823	[0.007, 0.181]*	[0, 5.73]	[0.477, 1.845]	0.006	0.002
AML-356	7	1	0.093	1.380	1.276	($-\infty$, 0.838]	(0, 17.703]	[0.629, 3.247]	-	-
AML-356	7	2	0.070	1.038	0.491	[0.028, 0.134]*	[0.051, 2.668]	[0.284, 1.143]	0.116	0.027
AML-356	7	3	0.071	0.476	2.333	($-\infty$, ∞)	(0, 12.867]	[1.465, 3.581]	0.005	0.014
AML-388	1	1	0.031	0.860	0.016	[0.025, 0.036]*	[0.774, 0.947]	[0.008, 0.061]	-	-
AML-388	1	2	0.067	0.367	0.275	[0.005, ∞)*	[0, 1.068]	[0.159, 0.649]	0.021	0.175
AML-388	1	3	0.025	1.502	0.030	[0.017, 0.034]*	[1.283, 1.731]	[0.014, 0.116]	-	-
AML-388	2	1	0.016	0.911	0.006	[0.014, 0.018]*	[0.877, 0.946]	[0.003, 0.023]	-	-
AML-388	2	2	0.026	1.022	0.172	($-\infty$, 0.005, 0.06]	[0.516, 1.612]	[0.099, 0.403]	0.015	0.286
AML-388	2	3	0.043	1.115	0.420	($-\infty$, 0.027, 0.137]	[0.076, 2.751]	[0.243, 0.988]	0.143	0.032
AML-388	3	1	0.136	1.123	0.426	[0.034, 0.343]*	[0.001, 4.394]	[0.207, 1.584]	-	-
AML-388	3	2	0.080	1.175	0.264	[0.042, 0.127]*	[0.416, 2.155]	[0.152, 0.621]	0.007	0.049
AML-388	3	3	0.080	1.011	0.334	[0.031, 0.147]*	[0.207, 2.164]	[0.193, 0.783]	0.002	0.028
AML-388	4	1	-0.003	2.564	0.030	($-\infty$, 0.011, 0.005]	[2.294, 2.889]	[0.014, 0.115]	-	-
AML-388	4	2	0.097	0.569	0.880	($-\infty$, -0.452] \cup [-0.049, ∞)	(0, 3.751]	[0.51, 1.898]	0.341	0.408
AML-388	4	3	0.065	1.444	0.177	[0.022, 0.117]*	[0.401, 2.84]	[0.085, 0.686]	-	-
AML-388	5	1	0.080	1.120	0.437	[0.018, 0.17]*	[0.107, 2.785]	[0.253, 1.022]	0.020	0.064
AML-388	5	2	0.033	1.087	0.136	[0.01, 0.058]*	[0.666, 1.562]	[0.078, 0.319]	0.064	0.023
AML-388	5	3	0.016	0.875	0.081	($-\infty$, 0.015, 0.049]	[0.456, 1.355]	[0.039, 0.314]	-	-
AML-388	7	1	0.080	1.141	0.383	[0.025, 0.158]*	[0.162, 2.614]	[0.222, 0.9]	0.032	0.120
AML-388	7	2	0.047	0.843	0.159	[0.019, 0.079]*	[0.426, 1.329]	[0.092, 0.375]	0.004	0.036
AML-388	7	3	0.076	2.477	0.320	[0, 0.177]*	[0.156, 6.529]	[0.155, 1.242]	-	-

Appendix B Complementary figures

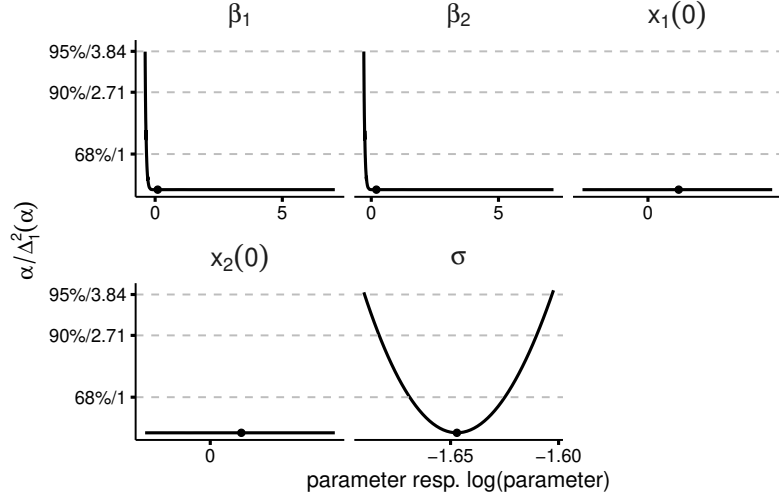


Fig. 7: Profile likelihoods for $\boldsymbol{\theta}^{(e)} = (\beta_1, \beta_2, x_1(0), x_2(0), \sigma)$ of the exponential growth model, where $x_1(0)$, $x_2(0)$ and σ are log-transformed, for simulated data with $\boldsymbol{\theta}^{(e)} = (0.1, 0.2, 10, 10, 0.2)$, showing that all parameters are structurally non-identifiable except σ

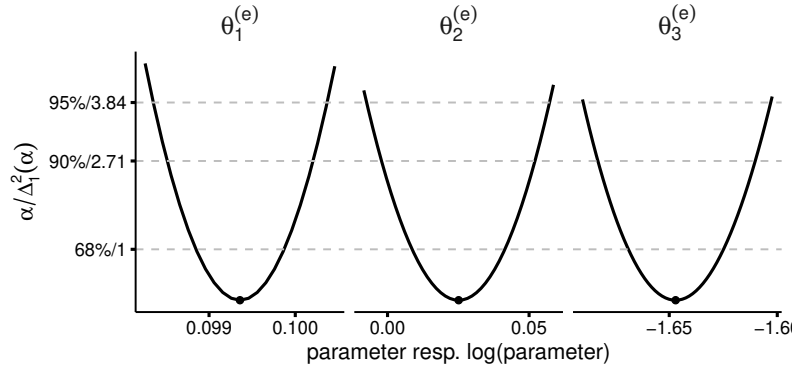


Fig. 8: Profile likelihoods for $\boldsymbol{\theta}^{(e)} = (\theta_1^{(e)}, \theta_2^{(e)}, \theta_3^{(e)})$ of the reparametrised exponential growth model, where $\theta_2^{(e)}$ and $\theta_3^{(e)}$ are log-transformed, based on the same data set as for Figure 7 in Appendix B, showing a structurally identifiable model parametrisation

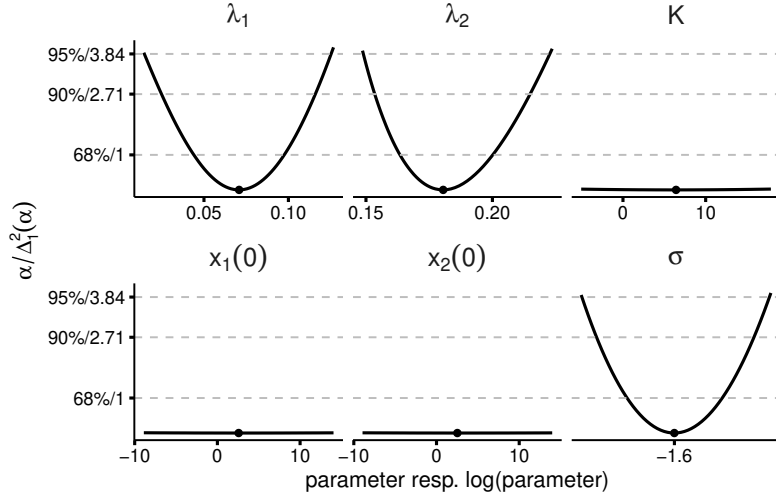


Fig. 9: Profile likelihoods for $\theta^{(l)} = (\lambda_1, \lambda_2, K, x_1(0), x_2(0), \sigma)$ of the logistic growth model, where K , $x_1(0)$, $x_2(0)$ and σ are log-transformed, for simulated data with $\theta^{(l)} = (0.1, 0.2, 1000, 10, 10, 0.2)$, showing that K , $x_1(0)$ and $x_2(0)$ are structurally non-identifiable

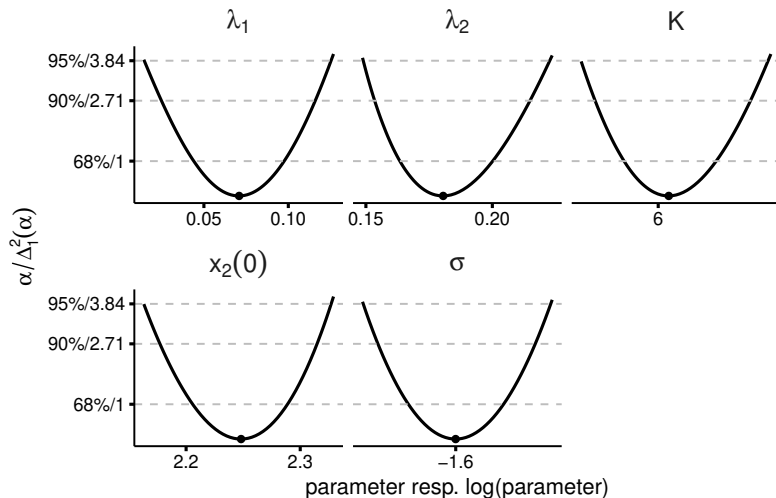


Fig. 10: Profile likelihoods for $\theta^{(l)}$ of the logistic growth model, where K , $x_2(0)$ and σ are log-transformed and $x_1(0) = 10$ is fixed, based on the same data set as for Figure 9 in Appendix B, showing a structurally identifiable model parametrisation

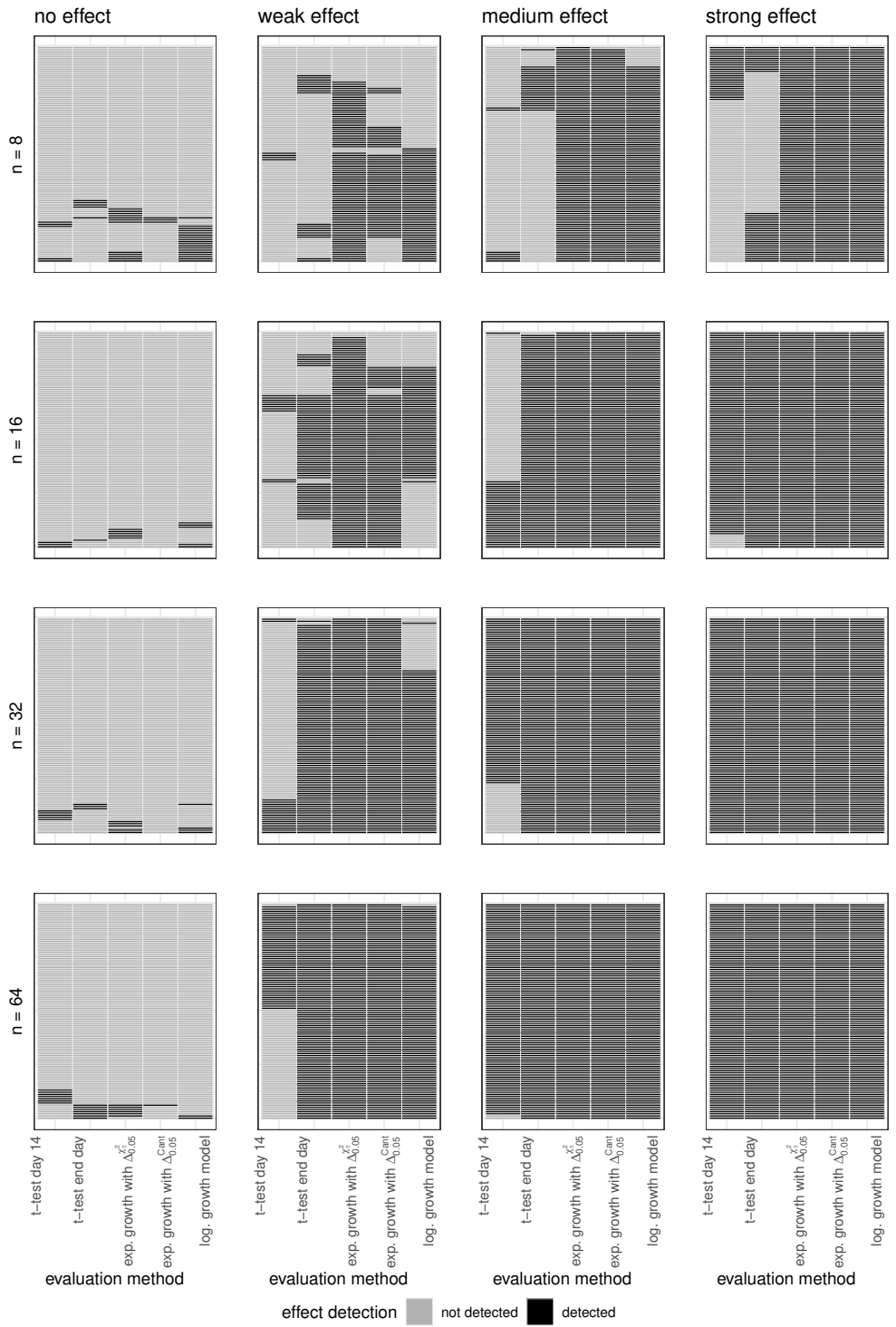


Fig. 11: More detailed presentation of detection results from Figure 5: while the other figure displays accumulated numbers of detected effects per evaluation method and sample size, this plot reveals the (dis-)agreement between evaluation methods for each of the 100 datasets. The evaluation results are displayed in the rows of the corresponding subplot. Recognised growth-altering effects in data sets are marked in black. If no effect is detected, the data set is marked in grey

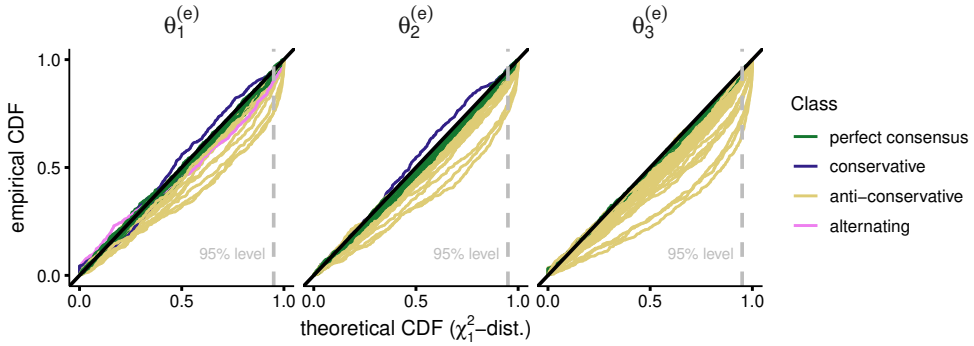


Fig. 12: Probability-probability plots (pp-plots) of the components of the parameter vector $\theta^{(e)}$ of the exponential growth model for all 44 knockout experiments in PDX models, showing that only about 37 % of the pp-plots are assigned to the perfect consensus region or the conservative class. At a confidence level of 0.95, the graphs of 54 % of all pp-plots lie in the perfect consensus region or in the conservative class

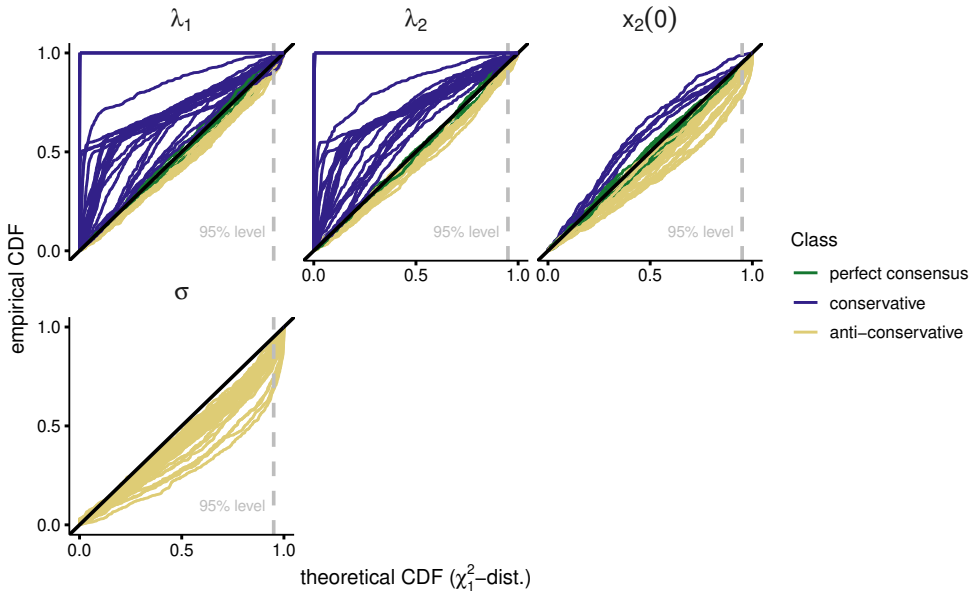


Fig. 13: Probability-probability plots (pp-plots) of the components of the parameter vector $\theta^{(l)}$ of the logistic growth model for all 44 knockout experiments in PDX models while keeping K and $x_1(0)$ fixed. Most pp-plots of λ_1 and λ_2 are assigned to the perfect consensus region or to the conservative class. More than half of the pp-plots of $x_2(0)$ and σ are assigned to the anti-conservative class. These overall classifications mostly coincide with the classifications at a confidence level of 0.95

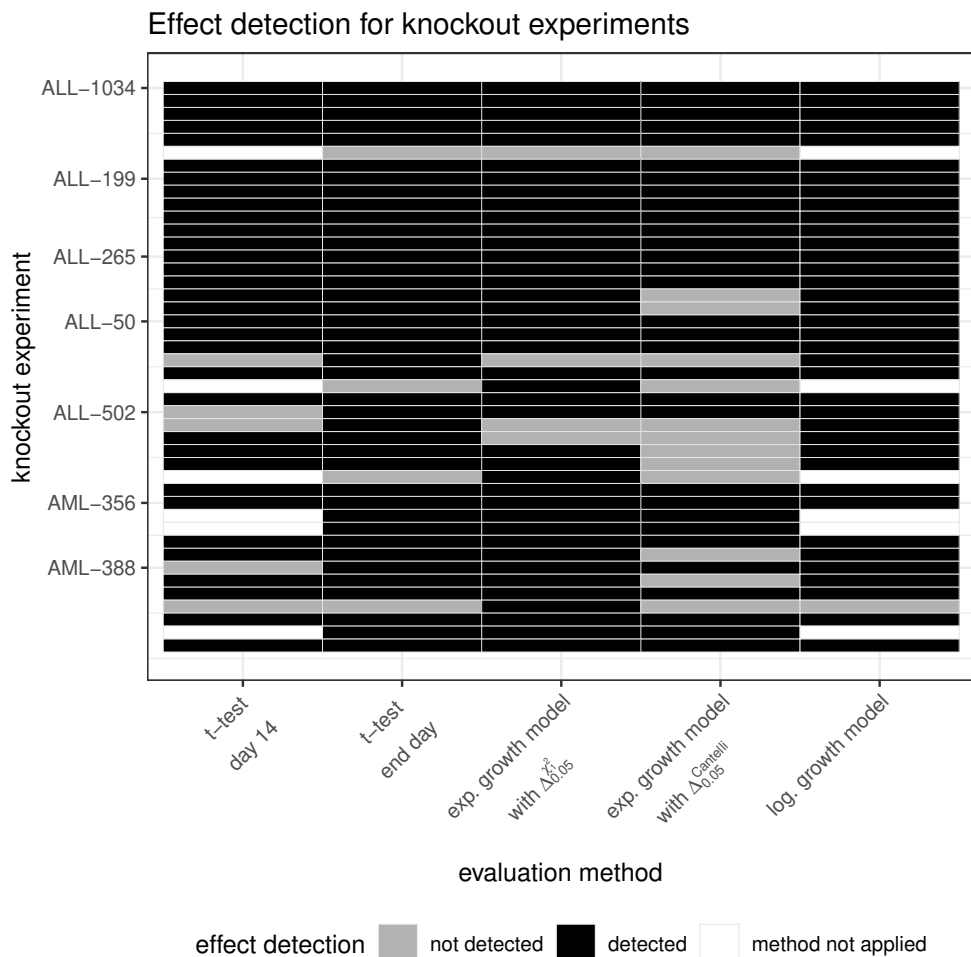


Fig. 14: More detailed presentation of detection results from Table 2: while the table displays accumulated numbers of detected effects for knockout experiments in PDX models via five evaluation methods, this plot reveals the (dis-)agreement between evaluation methods for each dataset. The experiments are arranged in rows as shown in Table 3 in Appendix A, i. e. in ascending order according to the gene numbers for each leukaemia sample considered. Experiments for which significant growth-altering effects are recognised based on an evaluation method are marked in black. If no effect is detected, the experiment is marked in grey. If the sample size of an experiment is too small to apply a method, it is marked in white